Coordination Chemistry Reviews 458 (2022) 214427

Contents lists available at ScienceDirect

Coordination Chemistry Reviews

journal homepage: www.elsevier.com/locate/ccr

Review

Core-shell structured nanoparticles for photodynamic therapy-based cancer treatment and related imaging

Yang Yang [a,c,1], Zhuotong Zeng [b,1], Eydhah Almatrafi [d,1], Danlian Huang [a], Chen Zhang [a], Weiping Xiong [a], Min Cheng [a], Chengyun Zhou [a], Wenjun Wang [a], Biao Song [a], Xiang Tang [a], Guangming Zeng [a,b,d,*], Rong Xiao [b,*], Zhi Li [c,*]

[a] College of Environmental Science and Engineering and Key Laboratory of Environmental Biology and Pollution Control (Ministry of Education), Hunan University, Changsha 410082, PR China
[b] Department of Dermatology, Second Xiangya Hospital, Central South University, Changsha 410011, PR China
[c] Department of Chemical and Materials Engineering, University of Alberta, Edmonton, Alberta T6G 1H9, Canada
[d] Center of Research Excellence in Renewable Energy and Power Systems, Center of Excellence in Desalination Technology, Department of Mechanical Engineering, Faculty of Engineering-Rabigh, King Abdulaziz University, Jeddah 21589, Saudi Arabia

ARTICLE INFO

Article history:
Received 1 December 2021
Accepted 17 January 2022
Available online 9 February 2022

Keywords:
Core-shell
Photodynamic therapy
Cancer treatment
Synergistic therapy
Imaging

ABSTRACT

Photodynamic therapy (PDT) is an emerging noninvasive therapy modality for treating cancer diseases. However, conventional PDT suffers from poor stability of organic photosensitizers, limited tissue penetration depth of excitation light and hypoxic tumor microenvironment, which hinders its modern clinical applications. The combination of PDT and nanotechnology is becoming a promising technology to tackle these troubles. Core-shell structured nanoparticles are of great interest as they can integrate the functionalities of individual components into one structure and exhibit improved physical and chemical properties that are different from the single component. Therefore, many efforts have been paid to develop core–shell structured nanoparticles for PDT of cancer. This review provides a panorama of the latest achievement in the developments of core–shell structured nanoparticles for PDT-based cancer treatment and related imaging. Concretely, this review starts with the categories of core–shell structured nanoparticles, followed by the functions of these nanoparticles in PDT of cancer, including photosensitizer delivery vehicle, energy transducer, photosensitizer and hypoxic tumor microenvironment modulator. Then the applications of core–shell structured particles for photodynamic synergistic therapy of cancer are highlighted as well as their imaging applications as contrast agents. Finally, perspectives on the major challenges and opportunities are presented for better developments in the future research.

Contents

* Corresponding authors at: College of Environmental Science and Engineering, Hunan University, Changsha 410082, PR China.
E-mail addresses: zgming@hnu.edu.cn (G. Zeng), xiaorong65@csu.edu.cn (R. Xiao), zhi.li@ualberta.ca (Z. Li).
[1] These authors contribute equally to this article.

https://doi.org/10.1016/j.ccr.2022.214427
0010-8545/

1. Introduction

Cancer, a disease that poses serious threats to the health of human beings, is becoming one of the leading causes of death globally. In 2020, nearly 19.3 million new cancer cases were diagnosed, and about 10.0 million cancer cases deaths occurred [1]. Due to the high risk and mortality of cancer, researchers all over the world have been working to develop effective therapies to treat cancer [2–4]. Conventional cancer therapies mainly include surgery, chemotherapy and radiotherapy, and they have some inescapable shortcomings. For example, surgery usually requires the cooperation of chemotherapy or radiotherapy to completely remove the cancer cells, and some tumors may recur after surgery [5,6]. Chemotherapy inhibits the cell division, leading to some side effects, such as alopecia and myelosuppression [7,8]. Besides, radiotherapy is restricted by the radiation site and cumulative radiation dose [9,10]. Accordingly, although improvement of the traditional cancer therapy modalities is important, it is also necessary to develop alternate therapy modalities that are safer, more effective and more affordable.

Photodynamic therapy (PDT) is an ideal cancer treatment method that can kill cancer cells through reactive oxygen species (ROS) generated by a photosensitizer under light irradiation [11,12]. Compared with traditional cancer treatment methods, PDT has the advantages of high safety, good repeatability, low long-term morbidity and high life quality of patients [13–15]. Normally, PDT consists of three essential components: photosensitizer, excitation light and molecular oxygen (O_2) [16]. These components are not toxic alone, but together they will trigger a photochemical reaction to produce cytotoxic ROS. Under the irradiation of light with a specific wavelength, photosensitizer can be excited and then react with substrates and O_2 to generate free radicals, such as superoxide radical ($\cdot O_2^-$) and hydroxyl radical ($\cdot$OH) (type I reaction). Alternatively, the excited photosensitizer can directly transfer its energy to O_2 to form highly reactive singlet oxygen ($^1O_2$), resulting in the significant cellular toxicity (type II reaction) [17]. Notably, three interrelated mechanisms are involved in the tumor destruction by PDT: direct tumor cell kill, vascular damage and immune response [11]. Since the significant breakthrough made in 1975 by Dougherty and co-workers [18], PDT has been proved to be effective in treating various cancers, such as skin cancer, head and neck cancers, and superficial bladder cancer.

Despite the extensive research and rapid growth, photodynamic cancer therapy still has some limitations in the modern clinical applications [19–21]. Typically, the traditional small organic molecule photosensitizers present poor stability and low targeting ability, which will reduce the efficiency of PDT and may evoke serious side effects [22,23]. The excitation wavelength of most photosensitizers is in the visible light region, which will result in the limited tissue penetration depth and thus hinder the wide application of PDT [24]. Moreover, the hypoxic tumor microenvironment induced by O_2 consumption will also affect the sustained effect of PDT [25,26]. In recent years, the introduction of nanoparticles into PDT has become a promising strategy to resolve these issues [27–29]. Among the various types of nanoparticles, the core–shell structured nanoparticles have stimulated great research interest as they can integrate the functionalities of individual components into one structure and exhibit improved physical and chemical properties that are different from the single component [30–32]. Meanwhile, the active interfaces between different components in core–shell structured nanoparticles may produce synergistic effects and novel properties [33,34]. For example, some biomolecules shells could not only stabilize the photosensitizers in biological fluids and extend their blood circulation time, but also provide the ability to actively target tumor sites [35–37]. The lanthanide-doped upconversion nanoparticles (UCNPs) cores could absorb near-infrared (NIR) light and convert it to ultraviolet–visible (UV–VIS) light, thereby exciting the photosensitizers loaded in the shells [38–40]. Compared with the UCNPs/metal–organic frameworks (MOFs) nanocomposite with Janus structure, the distance between UCNPs and MOFs in core–shell structured UCNPs@-MOFs nanoparticle is shorter, which could enhance the energy transfer efficiency from the UCNPs to the MOFs under NIR light irradiation, thus promoting the $^1O_2$ generation and improving the PDT efficacy [41–43]. Most importantly, the incorporation of functional materials or agents could enable core–shell structured nanoparticles to be multifunctional nanoplatforms for synergistic therapy and imaging [44–46]. These unique core–shell structured nanoparticles have been widely applied in photodynamic cancer therapy, but lacking a systematic understanding and overview.

This review aims to summarize the recent progress of core–shell structured nanoparticles in PDT-based cancer treatment and related imaging. First, the categories of core–shell structured nanoparticles are introduced according to the material compositions of the core and shell. Second, the functions of core–shell structured nanoparticles in PDT of cancer are comprehensively summarized. Then the achievements of core–shell structured nanoparticles in photodynamic synergistic therapy of cancer are discussed in detail. Additionally, the applications of core–shell structured nanoparticles in imaging during the PDT-based cancer treatment are mentioned. Ultimately, a brief conclusion and some perspectives on the future developments of this area are presented.

2. Categories of core–shell structured nanoparticles

In the past decades, various strategies have been developed to prepare core–shell structured nanoparticles because of the great application potentials of core–shell structures in many fields, such as biomedicine [47,48], energy utilization [49,50], catalysis [51,52], etc. Meanwhile, there are some excellent reviews that have

Table 1
Categories of core–shell structured nanoparticles in PDT of cancer.

Nanoparticle	Morphology	Synthesis methods		Functions	Ref.
		Core	Shell		
Class I: Inorganic core–shell structured nanoparticles					
UCNPs@$mSiO_2$	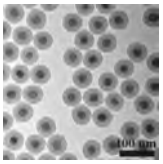	Thermal decomposition method	Sol-gel method	Photosensitizer (RB) delivery vehicle Energy transducer	[37]
UCNPs@$mSiO_2$	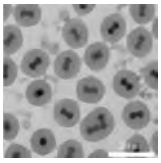	Coprecipitation method	Sol-gel method	Photosensitizer (ZnPc) delivery vehicle Energy transducer	[56]
AuNR@SiO_2	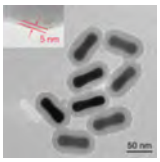	Seed-mediated growth method	Sol-gel method	Photosensitizer (HB) delivery vehicle	[57]
Fe_3O_4@SiO_2@$mSiO_2$	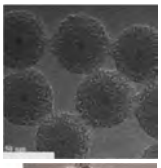	Solvothermal method	Sol-gel method	Photosensitizer (AlC_4Pc) delivery vehicle	[58]
UPCNs@TiO_2	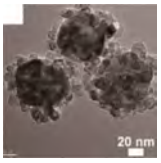	Thermal decomposition method	Solvothermal method	Energy transducer Photosensitizer (TiO_2)	[59]
SiO_2@MnO_2	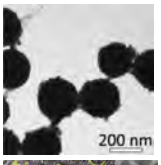	Sol-gel method	Reduction method	Photosensitizer (MB) delivery vehicle Hypoxic tumor microenvironment modulator	[60]
$Cu_{2-x}S$@MnS	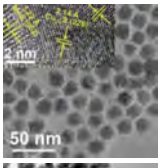	One-pot hot-injection method		Photosensitizer ($Cu_{2-x}S$) Hypoxic tumor microenvironment modulator	[61]
UCNPs@CaF_2	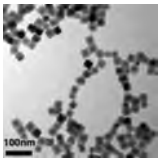	Thermal decomposition method	Epitaxial growth method	Photosensitizer (PpIX) delivery vehicle Energy transducer	[62]
Class II: Organic core–shell structured nanoparticles					
BDPVDA@mPEG-PPDA	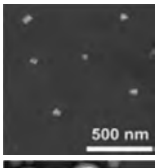	Self-assembly method		Photosensitizer (BODIPY)	[63]
Oil@lipid	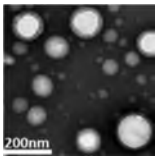	Sonication method		Photosensitizer (porphyrin-lipid)	[64]

(*continued on next page*)

Table 1 (*continued*)

Nanoparticle	Morphology	Synthesis methods		Functions	Ref.
		Core	Shell		
PFTBA@HSA		Ultrasonic emulsification method		Photosensitizer (IR780) delivery vehicle	[65]
RC@PDA	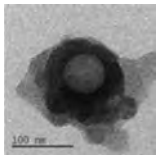	Solvent exchange and nucleation	Self-oxidation and polymerization	Photosensitizer (Ce6) delivery vehicle	[66]
Class III: Hybrid core–shell structured nanoparticles					
Au@PDMS-PEG	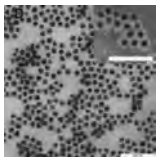	Reduction method	Hydrosilylation method	Photosensitizer (HB) delivery vehicle	[35]
Au@PDA	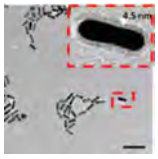	Seed-mediated growth method	Polymerization method	Photosensitizer (DSBDP) delivery vehicle	[67]
Ag@PANI	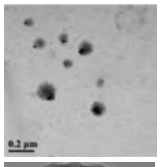	Reduction method	Polymerization method	Photosensitizer (ICG) delivery vehicle	[68]
Fe_3O_4@COFs	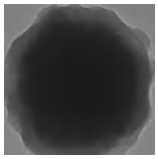	Solvothermal method	Templated method	Photosensitizer (COFs)	[69]
UCNPs@g-C_3N_4	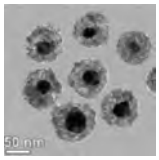	Thermal decomposition method	Polymerization method	Energy transducer Photosensitizer (g-C_3N_4)	[70]
PDA@UCNPs	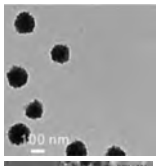	Polymerization method	Coprecipitation method	Photosensitizer (Ce6) delivery vehicle Energy transducer	[71]
SPN@MnO_2	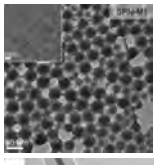	Precipitation method	Reduction method	Photosensitizer (PCPDTBT) Hypoxic tumor microenvironment modulator	[72]
AuNR@MOFs	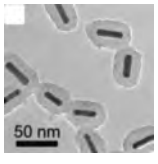	Seed-mediated growth method	Solvothermal method	Photosensitizer (MOFs)	[73]

Table 1 (*continued*)

Nanoparticle	Morphology	Synthesis methods		Functions	Ref.
		Core	Shell		
UCNPs@MOFs	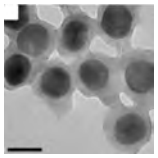	Thermal decomposition method	Precipitation method	Energy transducer Photosensitizer (MOFs)	[42]
ZIF-67@ZIF-8	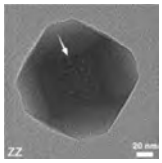	Precipitation method	Precipitation method	Photosensitizer (PpIX) delivery vehicle Hypoxic tumor microenvironment modulator	[74]

summarized the synthesis of core–shell structured nanoparticles in detail [53–55]. Therefore, here we do not intend to provide a repeated summary on the synthesis of core–shell structured nanoparticles, but rather to briefly introduce the categories of core–shell structured nanoparticles in PDT of cancer (Table 1). Broadly, a core–shell structured nanoparticle is composed of an inner core and an outer shell. According to material compositions of the core and shell, core–shell structured nanoparticles can be classified into three categories: inorganic, organic and hybrid.

2.1. Inorganic core–shell structured nanoparticles

Inorganic core–shell structured nanoparticles are the most important kind of the three types. The cores of the inorganic core–shell structured nanoparticles used for PDT of cancer are usually made of UCNPs [75,76], metals [77,78], metal oxides [79,80] and sulfides [81,82], while their shells are mainly composed of SiO_2 [75,79,82], metal oxides [76,81] and sulfides [61,83], and CaF_2 [62,84]. Notably, the SiO_2 coating can endow inorganic cores with low bulk conductivity and high suspension stability [53,85]. Moreover, because of the controllable pore structure, feasible functionalization and excellent biocompatibility, the coated SiO_2 shell can serve as a carrier to deliver photosensitizers [86,87]. Therefore, as a typical shell material, the SiO_2 has attracted much interest in recent years. For example, to avoid the shift of surface plasmon resonance (SPR) peak of gold nanorods (AuNR) from NIR region to visible light region, Qin et al. deposited a mesoporous SiO_2 ($mSiO_2$) shell on the surface of AuNR for preventing their aggregation under NIR laser irradiation [57]. After incorporating a hypocrellin B (HB) photosensitizer into the $mSiO_2$ shell, the AuNR@$mSiO_2$-HB nanoparticles presented great potential in synergistic PDT/photothermal therapy (PTT). In the study of Xu et al., a $NaGdF_4$:Yb, Er@$NaGdF_4$:Nd,Yb core was coated with a $mSiO_2$ shell containing dual-photosensitizer for PDT [88]. The chlorin e6 (Ce6) and merocyanine 540 (MC540) photosensitizers were loaded into the $mSiO_2$ shell through covalent bond and electrostatic interaction, respectively. As a consequence, the $mSiO_2$ shell not only enabled the nanoparticles to have a high photosensitizer loading, but also avoided the direct contact between photosensitizers and cells in organism, thereby protecting them from the *in vivo* microenvironment.

Apart from SiO_2, metal oxides and sulfides including TiO_2 [89,90], ZnO [91], MnO_2 [92], CeO_2 [81], ZrO_2 [93], MnS [61] and FeS [83], and CaF_2 [94] have also been employed as the shell materials of inorganic core–shell structured nanoparticles for PDT of cancer. For example, TiO_2 is a desirable photosensitizer as it can be maintained for a long time in human body and is nontoxic and stable without light irradiation [95]. In the study of Hou et al., a TiO_2 shell was coated on the surface of $NaYF_4$:Yb, Tm@$NaGdF_4$:Yb core for PDT [59]. The direct contact between TiO_2 shell and UCNPs core could ensure the maximum energy transfer from UCNPs to TiO_2, thereby accelerating the production and release of ROS. MnO_2 has a high O_2 generation ability in acidic and H_2O_2-rich tumor microenvironment, making it a good candidate for alleviating tumor hypoxia and enhancing PDT efficacy [96]. Li et al. developed a core–shell structured nanoparticle consisted of a hollow mesoporous CuS core loaded with the Ce6 photosensitizer and a MnO_2 shell for PDT/PTT [97]. The MnO_2 shell not only acted as a modulator to effectively alleviate tumor hypoxia, but also served as a gatekeeper to prevent the premature release of loaded Ce6. ZrO_2 can be utilized in imaging-guided therapy owing to its excellent biocompatibility and effective imaging ability [98]. Feng et al. fabricated UCNPs@ZrO_2 nanoparticles to load Ce6 photosensitizer, doxorubicin (DOX) and tetradecanol for multimodal imaging-guided PDT/PTT/chemotherapy [93]. The hollow and mesoporous ZrO_2 shell endowed the UCNPs@ZrO_2 nanoparticles with superior drug delivery capacity and satisfactory computed tomography (CT) imaging performance. Moreover, the CaF_2 shell can strengthen the upconversion luminescent intensity of UCNPs core and prevent the leakage of rare earth ions in UCNPs core [99]. A core–shell structured $NaYF_4$:Yb,Er@CaF_2 nanoparticle was fabricated by Punjabi et al. for *in vivo* deep tumor PDT treatment [62].

2.2. Organic core–shell structured nanoparticles

Both cores and shells of organic core–shell structured nanoparticles are made of polymers or other organic materials. Owing to the good biodegradability and high drug encapsulation efficiency, they are widely applied to the controlled release of photosensitizers in PDT of cancer [100]. Meanwhile, encapsulating photosensitizers in these nanoparticles can significantly increase the dispersibility and stability of photosensitizers, thereby improving their pharmacokinetic characteristics [28]. In recent years, poly (ethylene glycol) (PEG), as a nontoxic, nonimmunogenic, nonantigenic and water soluble polymer, has been frequently employed to construct organic core–shell structured nanoparticles for PDT of cancer [63,101]. For example, Kim et al. conjugated a pheophorbide a (PhA) photosensitizer with methoxy PEG (mPEG) through disulfide bond to fabricate the core–shell structured mPEG-(ss-PhA)$_2$ nanoparticles for PDT [102]. The disulfide bond was broken in the intracellular reductive environment, thereby promoting the rapid release of PhA photosensitizer. An et al. constructed an organic core–shell structured nanoparticle by conjugating Ce6 photosensitizer with luminol chemiluminescence substrate and PEG for H_2O_2-triggered in situ PDT [103]. At a pathologically

relevant H_2O_2 concentration, the Ce6 photosensitizer was activated through chemiluminescence resonance energy transfer to generate $^1O_2$ for in situ PDT of tumors and repressing lung metastasis. Besides, lipids have also been used to fabricate organic core–shell structured nanoparticles for encapsulating photosensitizers in PDT of cancer. Cheng et al. encapsulated IR780 photosensitizer and perfluorocarbon by lipids to create organic core–shell structured nanoparticles for PDT [104]. In the study of Chang et al., porphyrin-lipid shell was utilized to stabilize the water/oil interface to develop organic core–shell structured nanoparticles for PDT/chemotherapy [64].

2.3. Hybrid core–shell structured nanoparticles

There are two typical forms of hybrid core–shell structured nanoparticles: inorganic core-organic shell and organic core-inorganic shell. Normally, the inorganic–organic core–shell structured nanoparticles applied in PDT are made of metals [67], metal oxides [105] and UCNPs [106,107] cores and polymers [67,106,107] and organic carbonaceous materials [105,108] shells. One of the advantages of coating the organic shell on the inorganic core is that it can improve the stability and biocompatibility of the inorganic core. Meanwhile, the organic shell has abundant functional groups, which enables further photosensitizers loading and surface modification [109–111]. For example, Tan et al. coated a polyaniline (PANI) shell on a Ag core and then loaded an indocyanine green (ICG) photosensitizer to prepare the core–shell structured ICG-Ag@PANI nanoparticles for PDT/PTT [68]. The cell viability could still be maintained at about 70% in the dark when the concentration of Ag@PANI nanoparticles was as high as 400 μg mL^{-1}, which indicated the good biocompatibility of Ag@PANI nanoparticles. Liu et al. fabricated a novel core–shell structured gold nanoprism@mesoporous organosilica nanoparticle to load zinc(II) phthalocyanine (ZnPc) photosensitizer for PDT/PTT [112]. Owing to the π-π stacking and hydrophobic interactions induced by the mesoporous organosilica shell, the loading of the ZnPc photosensitizer could be as high as 11.8 wt%. In the study of Feng et al., Fe_3O_4 was employed as the core to in situ grow the covalent-organic frameworks (COFs) shell for PDT/PTT [69]. Due to the excellent biocompatibility of COFs, the cell viability of Fe_3O_4@COFs nanoparticles in the dark remained about 80% at a high concentration of 800 μg mL^{-1}. Ultimately, the Fe_3O_4@COFs nanoparticles presented satisfactory capacity to kill cancer cells and inhibit tumor growth through the synergistic effect of PDT/PTT. The structure of organic–inorganic core–shell structured nanoparticles is just the reverse of the above type. Coating the inorganic shell on the organic core is beneficial to enhance the whole strength and wear resistance of the nanoparticles [53]. In the study of Zhu et al., a MnO_2 shell was coated on a semiconducting hybrid nanoparticles (SPN) core through an in situ growth strategy [72]. Compared with the uncoated SPN, the SPN@MnO_2 nanoparticles showed better PDT efficacy as it could produce more $^1O_2$ in the hypoxic and acidic tumor microenvironment.

Moreover, metal–organic frameworks (MOFs), as an emerging hybrid functional materials assembled from inorganic metal nodes and organic linkers, have been extensively utilized to fabricate core–shell structured nanoparticles for PDT of cancer owing to their large surface area, tunable pore structure, intrinsic biodegradability and excellent biocompatibility [113–115]. Notably, the porous structure of MOFs can not only prevent the aggregation of photosensitizers to reduce their self-quenching, but also promote the diffusion of ROS. In the study of Ren et al., a pH-responsive nanoparticle was prepared for PDT/chemotherapy by encapsulating a DOX drug and a protoporphyrin IX (PpIX) photosensitizer in a zeolitic imidazolate framework-67 (ZIF-67) core and a zeolitic imidazolate framework-8 (ZIF-8) shell, respectively [74]. The ZIF-8 shell degraded in weak acidic tumor microenvironment, triggering the prior release of PpIX. Then the ZIF-67 core rapidly catalyzed H_2O_2 to produce O_2, which was utilized by PpIX to generate ROS under laser irradiation for enhanced PDT. Meanwhile, the decomposition of ZIF-67 core induced the release of DOX for chemotherapy. Moreover, in the study of Liu et al., an O_2 self-evolving nanoparticle was fabricated through coating a Material of Institute Lavoisie-NH_2 (MIL) shell on a CeO_x core for PDT [116]. Benefiting from the encapsulation and protection of the MIL shell, the CeO_x@MIL nanoparticles presented more stable activity for generating ROS in complex tumor microenvironment.

3. Core-shell structured nanoparticles for PDT of cancer

Recently, core–shell structured nanoparticles have been extensively applied in PDT of cancer. They play four main functions in this treatment: photosensitizer delivery vehicles, energy transducers, photosensitizers and hypoxic tumor microenvironment modulators. Notably, most core–shell structured nanoparticles can simultaneously perform multiple functions.

3.1. Photosensitizer delivery vehicles

In general, most photosensitizers are organic small molecules, which are easy to self-aggregate in aqueous phase, leading to a decrease in PDT efficacy [22,117]. Accordingly, appropriate delivery vehicles are needed to enhance their stability and targeting ability in PDT of cancer. The development of nanotechnology enables nanoparticles with a core–shell structure to meet these demands, improving the selectivity of photosensitizers to cancer cells [118–120]. In this process, the photosensitizers are first encapsulated into the core–shell structured nanoparticles through physical adsorption and chemical bonding. After the core–shell structured nanoparticles reach the targeted cancer cells and are irradiated by the light with a specific wavelength, the embedded photosensitizers will be excited and produce a large amount of toxic ROS to kill the cancer cells [121,122].

In a core–shell structured nanoparticle, both the core and shell can be used to load photosensitizers for PDT of cancer. Particularly, mesoporous nanostructures with large pore volume and high surface area are extremely beneficial to the loading of photosensitizers [123,124]. For example, Qian et al. fabricated $NaYF_4$:Yb, Er@SiO_2@mSiO_2 nanoparticles for PDT of MB49 bladder cancer cells (Fig. 1a) [125]. Incorporating the ZnPc photosensitizer into the mSiO_2 shell prevented it from being degraded in the complex biological environment and accelerated the release of ROS. Zeng et al. constructed MnO_2@polydopamine (PDA)-folic acid (FA) nanoparticles in which the Ce6 photosensitizer was loaded into the hollow mesoporous MnO_2 core for PDT of breast cancer [126]. The PDA shell avoided the premature release of Ce6 in blood circulation, while after reaching the acidic tumor site, the Ce6 was released because of the destruction of PDA shell. Meanwhile, photosensitizers can self-assemble with other organic molecules to form core–shell structured self-delivery nanoparticles for PDT of cancer [127,128]. In the study of Liu et al., about 13.89% of the Ce6 photosensitizer was loaded into a core–shell structured nanoparticle, which was composed of a core formed by self-assembly of Ce6 and rapamycin as well as a MOFs shell loaded with catalase [129].

In addition, the targeting ability of core–shell structured nanoparticles is critical to deliver photosensitizers to tumor sites. There are two routes utilized for the controlled delivery: active and passive delivery. In the case of active targeting, the customized tumor-targeting ligands are introduced on the core–shell structured nanoparticles for recognizing target cell receptors to deliver

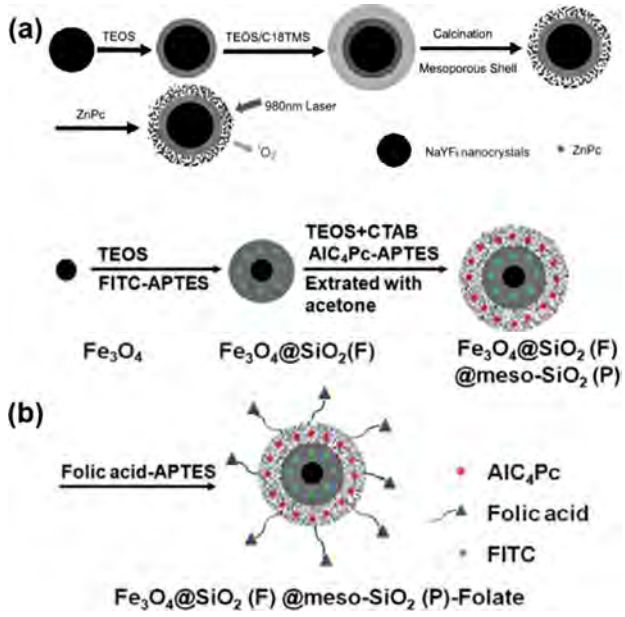

Fig. 1. (a) Schematic illustration of the synthesis of $NaYF_4$:Yb,Er@SiO_2@mSiO_2 nanoparticles. Reproduced with permission. [125] Copyright 2009, Wiley-VCH. (b) Schematic illustration of the synthesis of Fe_3O_4@SiO_2@mSiO_2-FA nanoparticles. Reproduced with permission. [58] Copyright 2011, Royal Society of Chemistry.

photosensitizers [130,131]. For example, folic acid (FA) exhibits a high affinity with folate receptor protein, which usually overexpresses on the surface of various cancer cells [132]. Wang et al. achieved superior cancer cell targeting ability in PDT by decorating the Fe_3O_4@SiO_2@mSiO_2 nanoparticles with FA (Fig. 1b) [58]. On the other hand, for passive targeting, the photosensitizers loaded core–shell structured nanoparticles will selectively accumulate in targeted cancer cells because of physicochemical or pharmacological factors [133]. Normally, in the case of passive targeting, most core–shell structured nanoparticles deliver photosensitizers based on the enhanced permeability and retention (EPR) effect [134,135]. In the study of Meng et al., owing to the high angiogenesis of triple-negative breast cancer, the CDTNs selectively accumulated in it via EPR effect, improving the PDT efficacy [136]. Wang et al. reported that the accumulation of FA modified core–shell structured poly (lactic-*co*-glycolic acid) (PLGA) nanoparticles in tumor was attributed to the synergistic effect of active targeting and EPR effect [137]. Overall, with the help of the delivery of core–shell structured nanoparticles, the photosensitizers can successfully reach the targeted cancer cells, thereby reducing damage to the surrounding healthy cells and enhancing PDT efficacy.

3.2. Energy transducers

Core-shell structured nanoparticles can not only serve as delivery vehicles for photosensitizers, but also act as energy transducers to excite photosensitizers. Since most traditional photosensitizers are excited by UV–VIS light that possesses limited tissue penetration depth, the clinical application of PDT is greatly hindered [117,138]. Combining these photosensitizers with core–shell structured nanoparticles with energy conversion properties is an effective way to solve this problem. In this process, the core–shell structured nanoparticles can convert the light with strong tissue penetration (e.g., NIR light and X-ray) to UV–VIS light for exciting the photosensitizers [24,139].

Among them, UCNPs are the most concerned, which can convert NIR light to UV–VIS light via an anti-Stokes emission process to excite photosensitizers for PDT of cancer [140–142]. Park et al. incorporated a Ce6 photosensitizer into the $NaYF_4$:Yb,Er@$NaGdF_4$ nanoparticles for PDT of U87MG tumor under NIR light irradiation [143]. When irradiated by a 980 nm NIR laser, the $NaYF_4$:Yb, Er@$NaGdF_4$ nanoparticles emitted red light, which was exploited to excite the Ce6 to produce cytotoxic $^1O_2$, resulting in the necrosis of U87MG tumor. In the study of Lucky et al., the $NaYF_4$:Yb, Tm@TiO_2-PEG nanoparticles exhibited admirable activity for PDT of human oral squamous cell carcinoma (OSCC) cells both *in vitro* and *in vivo* under 980 nm NIR laser irradiation [95]. In this system, electrons in the valence band (VB) of TiO_2 shell was excited to the conduction band (CB) because the $NaYF_4$:Yb,Tm core could convert NIR light to ultraviolet light (Fig. 2a). Consequently, the generation of charge carriers promoted the formation of ROS for killing the OSCC cells. Nevertheless, Yb^{3+}-sensitized UCNPs usually need to be excited by the 980 nm NIR light, which overlaps with the absorption of water molecules, leading to low tissue penetration depth and overheating of tissues [144,145]. Nd^{3+} doping can effectively solve this issue because it can tune the excitation wavelength of Yb^{3+}-sensitized UCNPs from 980 nm to around 800 nm where the tissue transparency is maximal and the heating effect is minimal [146–148]. For example, Xu et al. fabricated the dye-sensitized $NaGdF_4$:Yb,Er@$NaGdF_4$:Nd,Yb nanoparticles for dual-photosensitizer PDT of cancer upon 808 nm NIR laser excitation [88]. As displayed in Fig. 2b, it converted 808 nm photons to green and red light, thereby exciting the MC540 and Ce6 photosensitizers respectively to generate ROS for cancer therapy. As expected, the *in vitro* and *in vivo* tests demonstrated that the dye-sensitized $NaGdF_4$:Yb,Er@$NaGdF_4$:Nd,Yb nanoparticles possessed high efficacy for PDT of HeLa cancer cells and U14 tumors, respectively.

In addition to UCNPs, scintillator nanoparticles (SCNPs) are another promising energy transducers in PDT of cancer [149,150]. They present a high X-ray shielding capability and can convert X-ray to UV–VIS fluorescence [151,152]. For example, Zhang et al. prepared $LiYF_4$:Ce@SiO_2@ZnO nanoparticles for PDT of HeLa cancer cells under X-ray radiation [153]. As depicted in Fig. 2c, the $LiYF_4$:Ce core was excited by X-ray radiation and emitted ultraviolet fluorescence, which was utilized to induce the formation of photogenerated charge carriers in the ZnO shell. Subsequently, the photogenerated electrons and holes reacted with O_2 and H_2O to produce $\cdot O_2^-$ and ·OH respectively, thereby enhancing the antitumor therapeutic efficacy of PDT. Meanwhile, through the fluorescence resonance energy transfer (FRET) between SCNPs and photosensitizers, the SCNPs can efficiently realize deep PDT [154]. In the study of Hsu et al., $NaLuF_4$:Gd, Eu@$NaLuF_4$:Gd@$NaLuF_4$:Gd,Tb nanoparticles were designed for deep tissue PDT under X-ray radiation (Fig. 2d) [155]. Upon X-ray excitation, it emitted 543 nm green light (from Tb^{3+}), which overlapped with the main absorption peak of the loaded rose bengal (RB) photosensitizer (549 nm), allowing efficient FRET from the $NaLuF_4$:Gd,Eu@$NaLuF_4$:Gd@$NaLuF_4$:Gd,Tb donor to the RB acceptor. By virtue of the integral FRET system, a large amount of $^1O_2$ was produced to kill the MDA-MB-231 and MCF-7 cancer cells.

Notably, as variants of traditional core–shell structured nanoparticles, yolk-shell-like (core@void@shell) and hollow-like (void@shell) nanoparticles are considered to be beneficial for energy transfer in PDT due to the presence of internal cavity structures that facilitates light scattering [156–158]. For example, Wang et al. constructed UCNPs@$Zn_xCd_{1-x}S$ yolk-shell-like nanoparticles for PDT of HeLa cancer cells under 980 nm NIR laser irradiation [159]. The steady and dynamic fluorescence spectra demonstrated that the UCNPs@$Zn_xCd_{1-x}S$ yolk-shell-like nanoparticle was an efficient energy transducer for NIR light because it significantly enhanced the energy transfer efficiency. In the study of Chang et al., Au@CuS yolk-shell-like nanoparticles were developed for PDT/PTT/chemotherapy [160]. The yolk-shell structure could enhance local electromagnetic field to induce a resonance energy

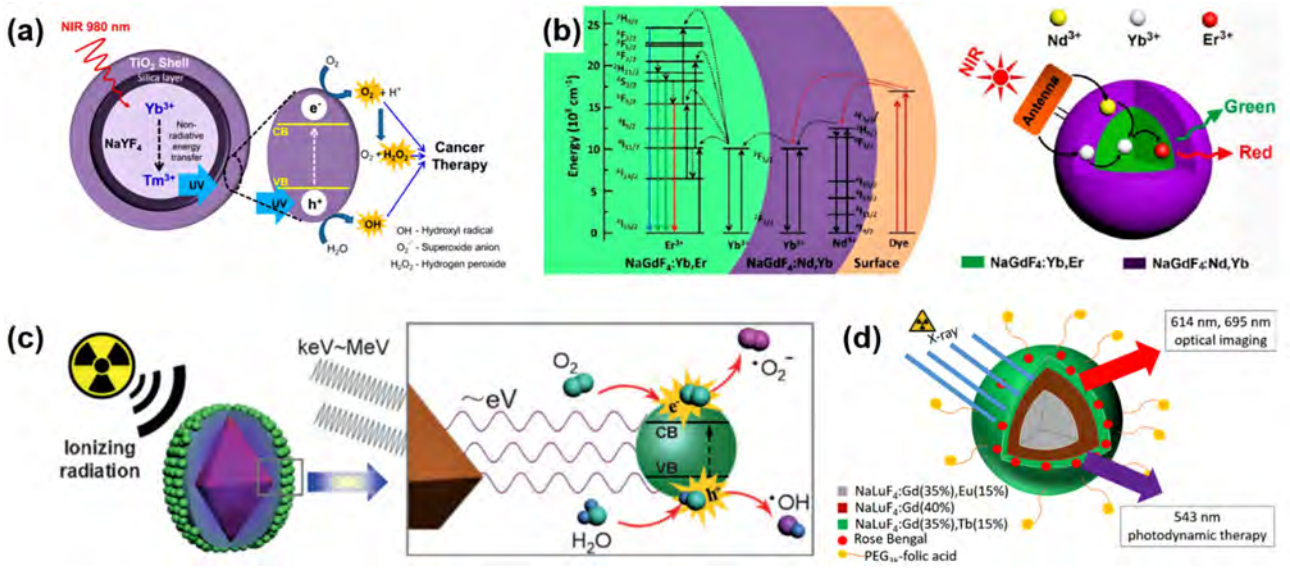

Fig. 2. (a) Mechanism of the $NaYF_4$:Yb,Tm@TiO_2-PEG nanoparticles in PDT of cancer under 980 nm NIR laser irradiation. Reproduced with permission. [95] Copyright 2015, American Chemical Society. (b) Proposed energy level diagram and energy-transfer mechanism in the dye-sensitized $NaGdF_4$:Yb,Er@$NaGdF_4$:Nd,Yb nanoparticles under 808 nm NIR laser irradiation. Reproduced with permission. [88] Copyright 2017, American Chemical Society. (c) Mechanism of the $LiYF_4$:Ce@SiO_2@ZnO nanoparticles in PDT of cancer under X-ray radiation. Reproduced with permission. [153] Copyright 2015, Wiley-VCH. (d) Energy-transfer mechanism in the $NaLuF_4$:Gd,Eu@$NaLuF_4$:Gd@$NaLuF_4$:Gd,Tb nanoparticles under X-ray radiation. Reproduced with permission. [155] Copyright 2018, American Chemical Society.

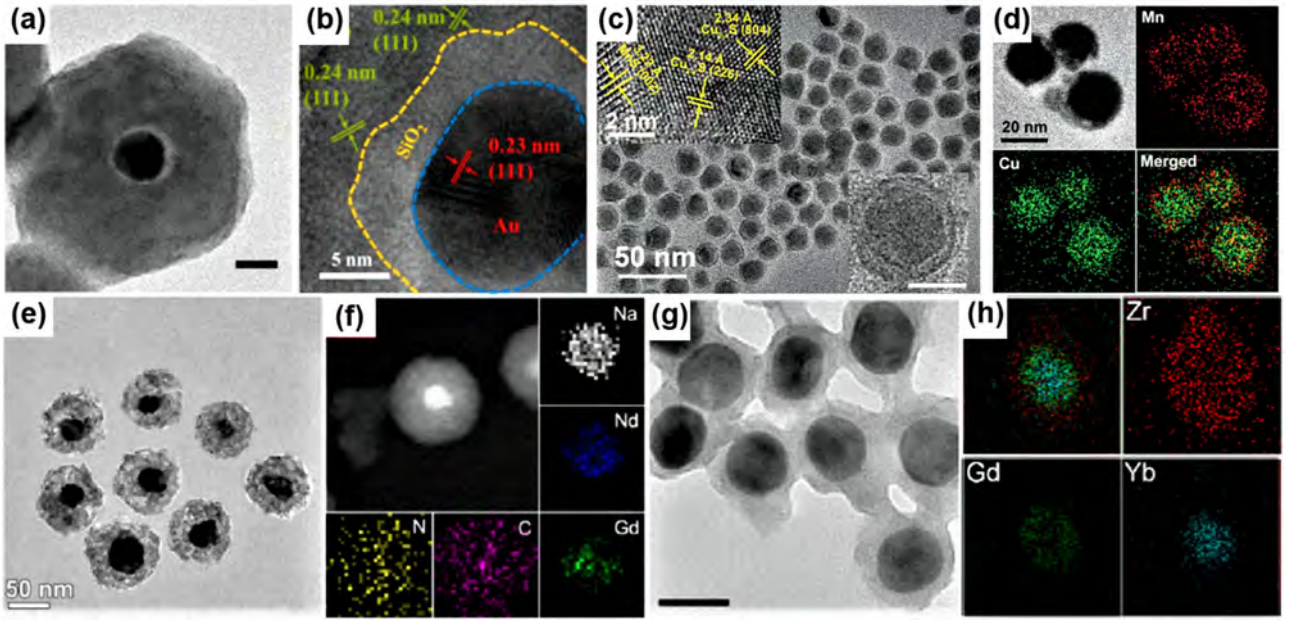

Fig. 3. (a) TEM image and (b) interfacial HRTEM image of the Au@SiO_2@Cu_2O nanoparticles. Reproduced with permission. [165] Copyright 2018, American Chemical Society. (c) TEM image and (d) EDS elemental mapping images of the $Cu_{2-x}S$@MnS nanoparticles. Reproduced with permission. [61] Copyright 2019, Wiley-VCH. (e) TEM image of the UCNPs@g-C_3N_4 nanoparticles, and (f) STEM image and EDS elemental mapping images of the UCNPs@g-C_3N_4-PEG nanoparticles. Reproduced with permission. [70] Copyright 2016, American Chemical Society. (g) TEM image and (h) EDS elemental mapping images of the UCNPs@porphyrinic MOFs nanoparticles. Reproduced with permission. [42] Copyright 2020, American Chemical Society.

transfer from Au core to CuS shell, improving both photodynamic and photothermal performance. As a result, under 980 nm NIR laser irradiation, it displayed excellent antitumor efficacy for *in vitro* 4 T1 cancer cells and *in vivo* 4 T1 tumor-bearing mice. Moreover, to obtain high energy transfer efficiency, Kamkaew et al. utilized the hollow $mSiO_2$ nanoparticles as a carrier to simultaneously encapsulate ^{89}Zr isotope and Ce6 photosensitizer [161]. In this system, ^{89}Zr isotope could serve as a Cerenkov radiation source to excite Ce6 photosensitizer to produce ROS for PDT of cancer.

3.3. Photosensitizers

Owing to the unique light absorption characteristics, some core–shell structured nanoparticles have the capability to produce ROS upon light excitation, which allows them to serve as photosensitizers in PDT by themselves. Metal oxide and sulfide semiconductors have attracted much attention as photosensitizers in PDT of cancer because of their efficient photoactivity [162–164]. Under light irradiation, they are induced to generate electron-hole pairs, which can react with O_2 and H_2O to produce various ROS for killing

the cancer cells. For example, Liu et al. constructed Au@SiO_2@Cu_2O nanoparticles (Fig. 3a and b) and loaded them into perfluorohexane droplets with liposome coating for PDT of cancer under 670 nm laser irradiation [165]. The process of plasmon-induced resonance energy transfer from Au core to Cu_2O shell facilitated the generation of charges in Cu_2O shell, resulting in a significant increase in the quantum yield of $^1O_2$. Hence this nanocomposite exhibited outstanding anticancer efficacy for *in vitro* MCF-7 cancer cells and *in vivo* MCF-7 tumor xenotransplanted BALB/c nude mice. Wang et al. integrated oxygen vacancy-enriched core–shell structured crystalline@amorphous black TiO_2 into a chitosan matrix for PDT of cancer [166]. Under 808 nm NIR laser irradiation, the thermogel showed considerable activity in killing B16F10 cells *in vitro* and inhibiting B16F10 tumors growth *in vivo*. Moreover, Huang et al. prepared $Cu_{2-x}S$@MnS nanoparticles (Fig. 3c and d) for PDT of HeLa cancer cells [61]. In this structure, the $Cu_{2-x}S$ core acted as a photosensitizer to generate ROS for PDT upon 808 nm NIR laser excitation.

Apart from metal oxide and sulfide semiconductors, graphitic carbon nitride (g-C_3N_4) also has been employed as a photosensitizer for PDT of cancer, which is ascribed to its low cytotoxicity, excellent biocompatibility, good photostability and low cost [167–171]. As exhibited in Fig. 3e and f, Feng et al. created UCNPs@g-C_3N_4-PEG nanoparticles for PDT of HeLa cells *in vitro* and U14 tumors *in vivo* under 808 nm NIR laser irradiation [70]. The UCNPs core converted absorbed NIR light to UV–VIS light, which could excite electrons in the VB of g-C_3N_4 shell to the CB and thus induce the formation of photogenerated electron-hole pairs. These photogenerated electrons and holes then reacted with O_2 and H_2O respectively to produce $\cdot O_2^-$ and ·OH, resulting in the death of HeLa cells and inhibition of U14 tumors growth. In the study of Zhang et al., the nitrogen-doped graphene quantum dot (N-GQD)@hollow $mSiO_2$@g-C_3N_4-amphipathic polymer (R-NCNP) nanoparticles presented superior anticancer effects both *in vitro* and *in vivo* [108]. In this nanocomposite, the g-C_3N_4 photosensitizer was excited by a 630 nm laser to produce ROS for PDT of cancer.

More recently, porphyrinic MOFs have shown great potential as photosensitizers for PDT of cancer [172–174]. Since porphyrinic MOFs are directly self-assembled by the coordination interactions between porphyrin photosensitizers and metal ions/clusters, the porphyrin-derived molecules are uniformly dispersed in the whole porphyrinic MOFs framework, which maximizes the light harvesting ability. Meanwhile, the abundant pore structures of MOFs accelerate the diffusion of ROS, thereby enhancing the PDT efficacy. For example, Zeng et al. reported that AuNR@porphyrinic MOFs nanoparticles exhibited excellent PDT efficacy upon NIR laser excitation for killing the cancer cells *in vitro* and inhibiting the tumor growth and metastasis *in vivo* [73]. In the study of Shao et al., UCNPs@porphyrinic MOFs (UCSs) nanoparticles (Fig. 3g and h) were constructed for PDT of hypoxic tumors [42]. Benefiting from the efficient energy transfer from UCNPs core to porphyrinic MOFs shell, the UCNPs@porphyrinic MOFs nanoparticles presented rapid generation of $^1O_2$ under 980 nm NIR laser irradiation, resulting in the enhanced PDT efficacy.

3.4. Hypoxic tumor microenvironment modulators

Hypoxia is a prominent feature of tumor microenvironment, which originates from the uncontrolled cancer cells growth and abnormal angiogenesis [175,176]. Moreover, the process of PDT also consumes O_2 to generate ROS, thereby exacerbating the tumor hypoxia [177,178]. Hypoxic tumor microenvironment not only accelerates the cancer metastasis but also impairs the therapeutic efficacy of PDT [179,180]. Recently, various core–shell structured nanoparticles have been developed to modulate hypoxic tumor microenvironment for attenuating the tumor hypoxia in PDT [181–184]. Normally, there are two main mechanisms in the process of utilizing core–shell structured nanoparticles to overcome this obstacle.

One mechanism is the direct transport of O_2 to hypoxic tumor areas through the core–shell structured nanoparticles to effectively oxygenate the tumor. Perfluorocarbon is an efficient O_2 carrier due to its high affinity toward O_2 molecules [65,185]. In the study of Cheng et al., the IR780 photosensitizer was loaded into an oxygen self-enriched nanoparticle, which was composed of perfluorocarbon droplet core and lipid shell [104]. In this nanoparticle, the IR780 photosensitizer was evenly dispersed inside the lipid shell. When irradiated by a 808 nm NIR laser, the IR780 transferred energy to the oxygen enriched-perfluorocarbon droplet core for cytotoxic $^1O_2$ production, leading to an enhanced tumor inhibition. However, perfluorocarbon-based O_2 carriers present a limited ability to transport O_2 to the tumor site. On account of the large pore volume and high surface area, MOFs have been regarded as promising candidates for O_2 storage and transport [186,187]. Xie et al. constructed a multifunctional nanoplatform by covalently conjugating DOX and NH_2-poly(ethylene glycol) modified folic acid on the surface of core–shell structured UCNPs@$mSiO_2$-RB@ZIF-90 nanoparticles for highly efficient cancer therapy under 808 nm NIR laser irradiation [188]. The outermost ZIF-90 shell was an O_2 reservoir, which decomposed under acidic conditions, enabling rapid release of O_2 at hypoxic tumor microenvironment. After the addition of UCNPs@$mSiO_2$-RB@ZIF-90 nanoparticles, the O_2 concentration in deoxygenated phosphate-buffered saline (PBS) solution at low pH value was increased.

Another mechanism is using core–shell structured nanoparticles with catalase-like properties to catalyze endogenous H_2O_2 for in situ O_2 production. Mn-based materials (e.g., MnO_2 [189], MnS [61] and Mn-Cdots [190], etc.) are the most commonly used catalase-like nanoenzymes to alleviate tumor hypoxia by virtue of their superior activity. For example, Zhu et al. developed a core–shell structured nanoparticle composed of a MnO_2 shell and a SPN core for enhanced PDT of 4 T1 cancer cells both *in vitro* and *in vivo* [72]. Under hypoxic and acidic tumor microenvironment, the MnO_2 shell decomposed H_2O_2 to O_2. Subsequently, the O_2 was activated by the SPN core under 808 nm NIR laser irradiation to form $^1O_2$ for cancer therapy. Compared with the uncoated SPN, the MnO_2 coated SPN (SPN-M1) produced 2.68-fold more $^1O_2$ at hypoxic and acidic conditions under NIR laser irradiation. Moreover, Huang et al. reported that the MnS shell in $Cu_{2-x}S$@MnS nanoparticles acted as a H_2O_2 responder to mediate O_2 production for efficiently relieving tumor hypoxia [61]. Nevertheless, Mn-based materials are only suitable for acidic tumor microenvironment since their catalytic activity is greatly affected by the pH. As an emerging catalase-like nanoenzyme, noble metals have drawn much attention due to their admirable stability and pH-independent activity [191–193]. For example, Wang et al. designed Pt-based core–shell structured nanoparticles to promote the decomposition of endogenous H_2O_2 for enhanced PDT efficacy (Fig. 4a-c) [194]. In this nanoparticle, the Pt interlayer first decomposed the endogenous H_2O_2 to O_2, which was then converted to cytotoxic $^1O_2$ by the zirconium-porphyrin (PCN) shell when exposed to light irradiation (Fig. 4f). As shown in Fig. 4d and e, the O_2 generation and $^1O_2$ production efficiencies over the polydopamine (Pda)-Pt@PCN nanoparticles were significantly enhanced. Meanwhile, cellular level tests further verified the O_2-generating capability and the improved $^1O_2$-producing capability of the Pda-Pt@PCN nanoparticles (Fig. 4g and h). In another study, a porous Au@Rh core–shell structured nanoparticle was developed to alleviate tumor hypoxia for improved PDT [78]. As expected, it showed excellent catalase-like activity to effectively decompose H_2O_2 to O_2 in tumors.

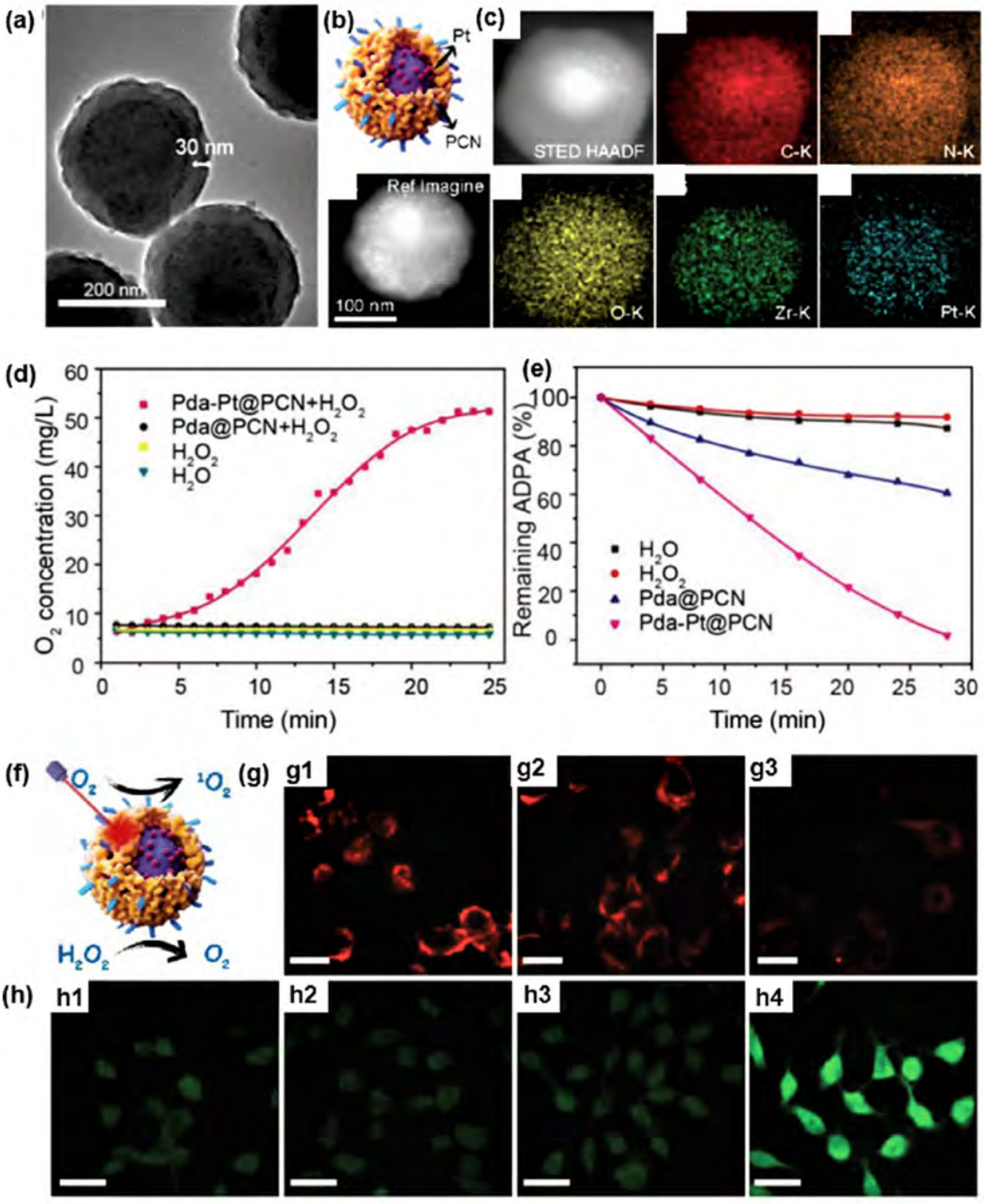

Fig. 4. (a) TEM image, (b) schematic illustration, (c) STEM-HAADF image and the corresponding element mapping images of the Pda-Pt@PCN nanoparticles. (d) O_2 generation and (e) $^1O_2$ production efficiencies over different samples. (f) Schematic illustration of O_2 generation and $^1O_2$ production over the Pda-Pt@PCN nanoparticles upon light excitation. (g) CLSM images of intracellular hypoxia levels in CT26 cells under 5% O_2 treated with (g1) blank, (g2) Pda@PCN-FA and (g3) Pda-Pt@PCN-FA. The scale bar is 36 μm. (h) CLSM images of ROS production in CT26 cells treated with (h1) 2′,7′-dichlorofluorescein diacetate in dark, (h2) 2′,7′-dichlorofluorescein diacetate under 660 nm LED irradiation, (h3) Pda-Pt@PCN-FA in dark and (h4) Pda-Pt@PCN-FA under 660 nm LED irradiation. The irradiation time was 2 min. The scale bar is 36 μm. Reproduced with permission. [194] Copyright 2018, Wiley-VCH.

Unfortunately, the amount of O_2 generated by catalase-like core–shell structured nanoparticles is highly dependent on the decomposition of endogenous H_2O_2, while the low level of endogenous H_2O_2 in tumor cells is not enough to produce a considerable amount of O_2 to alleviate tumor hypoxia [195]. To solve this problem, He et al. designed a UCNPs@MOFs(UMOFs)@Au cascade biocatalyst to continuously produce O_2 for PDT (Fig. 5a) [196]. Firstly, the ultrasmall Au nanoparticles first converted glucose to H_2O_2 in tumor microenvironment, leading to the increase of H_2O_2 concentration (Fig. 5b). Subsequently, the H_2O_2 was decomposed by the iron porphyrin MOFs shell through the catalase-like reaction to generate O_2 (Fig. 5c). Finally, the UCNPs core converted NIR light to visible light, thereby exciting the iron porphyrin MOFs shell to produce cytotoxic $^1O_2$ for cancer therapy. In addition, given the abundance and availability of endogenous H_2O in tumor microenvironment, Zhang et al. designed an intelligent

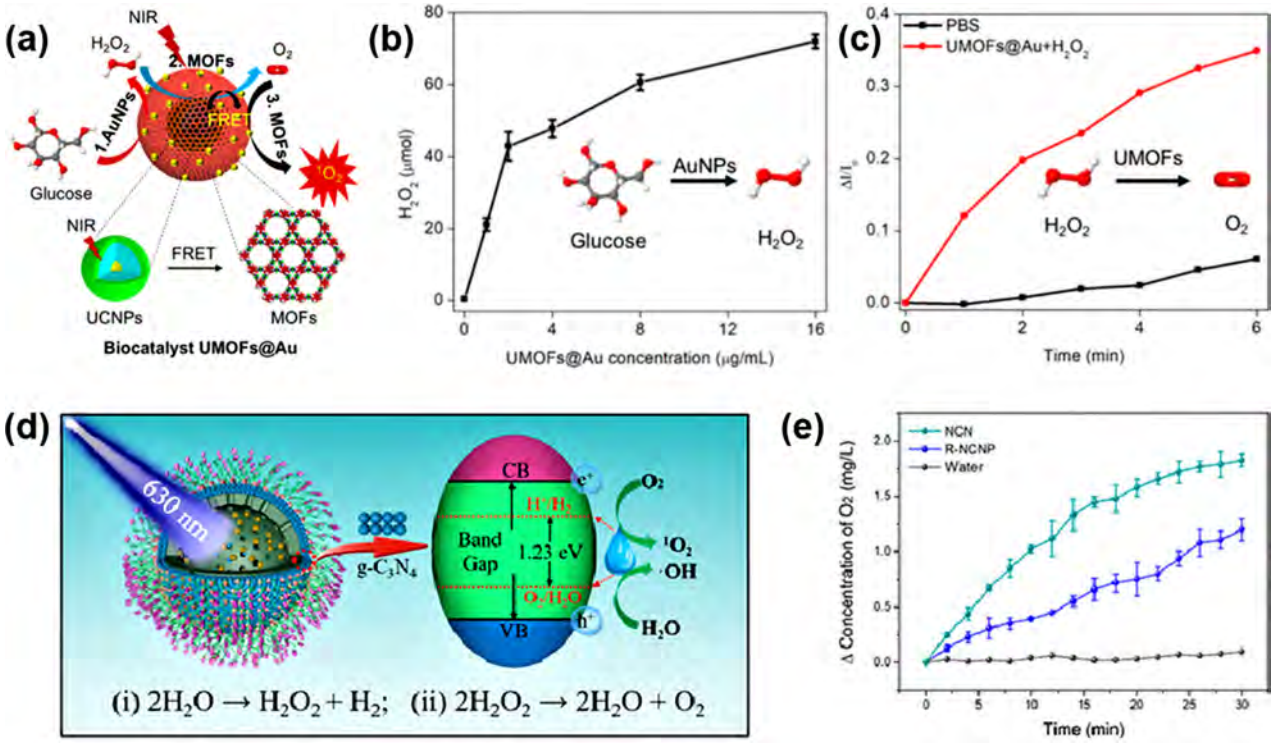

Fig. 5. (a) Schematic illustration of the UMOFs@Au cascade biocatalyst for PDT. (b) Concentration-dependent H_2O_2 generation and (c) time-dependent O_2 generation from the UMOFs@Au cascade biocatalyst. Reproduced with permission. [196] Copyright 2020, American Chemical Society. (d) Schematic illustration of the proposed R-NCNP nanoregulator for the light-driven water-splitting process and related reaction equations. (e) O_2 production curve of the R-NCNP nanoparticles in water solution. Reproduced with permission. [108] Copyright 2020, American Chemical Society.

nanoregulator (R-NCNP) to execute laser-excited water splitting for enhanced PDT (Fig. 5d) [108]. As shown in Fig. 5e, the g-C_3N_4 in R-NCNP split H_2O to O_2 under 630 nm laser irradiation, which was then converted to $^1O_2$ by the photosensitizers in R-NCNP, thereby efficiently attenuating tumor hypoxia and enhancing PDT efficacy.

4. Core-shell structured nanoparticles for photodynamic synergistic therapy of cancer

The combination of PDT with other therapies is beneficial to improve the anticancer efficacy [197,198]. On the one hand, photodynamic synergistic therapy can greatly avoid the side effects on healthy tissues through reducing the therapeutic dosage. On the other hand, it can tackle some of the challenging issues in monotherapy, such as metastasis of tumors and development of resistance. Core-shell structured nanoparticles are an ideal nanoplatform for photodynamic synergistic therapy on account of the convenience of incorporating functional materials or agents [55,199,200]. The applications of core–shell structured nanoparticles in photodynamic synergistic therapy of cancer are listed in Table 2. Herein, core–shell structured nanoparticles for photodynamic synergistic therapy of cancer are introduced according to the combination of PDT with different therapies (e.g., chemotherapy, PTT and immunotherapy).

4.1. PDT combined with chemotherapy

Chemotherapy is one of the most widely used cancer treatment strategies in the past few decades, which ingests chemotherapeutic drugs orally or intravenously to suppress tumor growth [209,210]. Although chemotherapy has the unique merits of eliminating cancer cells in the early stage and improving survival rate in the late stage, there are still some therapeutic limitations, such as premature drug release, severe drug resistance and side effects on healthy tissues [211,212]. The integration of chemotherapy and PDT into a single nanoparticulate system is a promising way to solve these issues [213–215]. Specifically, nanoparticulate system can promote the delivery of small molecule drugs to tumor sites via the EPR effect, resulting in the selective distribution of drugs and low toxicity to healthy tissues. What is more, chemotherapy can increase the sensitivity of tumor cells to photoinduced ROS, while ROS in turn can restrain the activity of proteins related to drug efflux, thereby reducing the possibility of drug efflux and restoring multidrug tolerance. Recently, the development of core–shell structured nanoparticles for cancer therapy by combining PDT with chemotherapy has attracted great interest to realize superior anticancer effect [74,181].

Normally, chemotherapeutic drugs can self-assemble with traditional small molecule photosensitizers to form core–shell structured nanoparticles for combined therapy of PDT/chemotherapy [216]. For example, He et al. reported a self-assembled nanoscale coordination polymer (NCP)@pyropheophorbide-lipid (pyrolipid) nanoparticle with cisplatin drug in the core and pyrolipid photosensitizer in the shell for PDT/chemotherapy [201]. As depicted in Fig. 6a, the NCP@pyrolipid kept structural integrity extracellularly, but released pyrolipid and cisplatin intracellularly, leading to the apoptosis and necrosis of cancer cells. Flow cytometry results demonstrated that the NCP@pyrolipid nanoparticles aroused the highest level of apoptosis (26.0%) and necrosis (14.5%) for SQ20B human head and neck cancer cells under 670 nm LED light irradiation (Fig. 6b). Pharmacokinetic and biodistribution investigations of the NCP@pyrolipid nanoparticles in CT26 tumor-bearing mice indicated that the pyrolipid and cisplatin presented low uptake in normal organs, high tumor accumulation and extended blood circulation times (Fig. 6c-f). By virtue of the

Table 2
Core-shell structured nanoparticles for photodynamic synergistic therapy of cancer and related imaging.

Nanoparticle	Excitation light	Modality	Objects		Imaging	Ref.
			In vitro	*In vivo*		
NCP@pyrolipid	LED (670 nm)	PDT/Chemotherapy	HNSCC135, SCC61, JSQ3 and SQ20B cells[a)]	SQ20B tumor-bearing mice	Optical	[201]
PTX-S-OA@PPa-PEG	Laser (660 nm)	PDT/Chemotherapy	KB[b)], 4T1[c)] and A549[d)] cells	KB tumor-bearing mice	Optical	[128]
Au@dsDNA/G4	Laser (690 nm)	PDT/Chemotherapy	HeLa cells	HeLa tumor-bearing mice	Optical	[120]
SAD@ZIF-90	Laser (808 nm)	PDT/Chemotherapy	HeLa cells	HeLa tumor-bearing mice	Optical	[114]
UCNPs@mSiO_2@ZIF-90	Laser (808 nm)	PDT/Chemotherapy	4T1 cells and HeLa cells	H22[e)] tumor-bearing mice	Optical/MR	[188]
AuNR@SiO_2	Laser (780 nm)	PDT/PTT	CT26[f)] cells	–	Optical	[77]
AuNR@MOFs	Laser (640 nm and 808 nm)	PDT/PTT	4T1 cells	4T1 tumor-bearing mice	Optical/Photothermal	[202]
b-P25@PDA-Ce6 (Mn)	Laser (671 nm and 808 nm)	PDT/PTT	4T1 cells	4T1 tumor-bearing mice	Optical/Photothermal/MR	[203]
TiO_2@RP	Laser (808 nm)	PDT/PTT	OS-RC-2 and 786-O cells[g)]	786-O tumor-bearing mice	Optical/Photothermal	[204]
HMCuS@MnO_2	Laser (660 nm and 808 nm)	PDT/PTT	4T1 cells	4T1 tumor-bearing mice	Optical/Photoacoustic/MR	[97]
ZnP@pyrolipid	Laser (670 nm)	PDT/Immunotherapy	4T1 cells	4T1 tumor-bearing mice	Optical	[205]
TPPM@BioPEGDMA	Laser (660 nm)	PDT/Immunotherapy	CT26 cells	CT26 tumor-bearing mice	Optical	[206]
$LiYF_4$:Ce@SiO_2@ZnO	X-ray	PDT/Radiotherapy	HeLa cells	HeLa tumor-bearing mice	–	[153]
PEG/LDNPs@CMSNs	Laser (980 nm)	PDT/CDT	HeLa cells	HeLa tumor-bearing mice	Optical/MR/CT	[207]
mSiO_2@MnO_2@PEG	Laser (808 nm)	PDT/CDT	4T1 cells	4T1 tumor-bearing mice	Optical	[92]
UCNPs@mSiO_2-CuS	Laser (980 nm)	PDT/PTT/ Chemotherapy	HeLa cells	H22 tumor-bearing mice	Optical/Photothermal/MR/CT	[208]
PDA@UCNPs	Laser (980 nm)	PDT/PTT/ Immunotherapy	4T1 cells	4T1 tumor-bearing mice	Optical/Photothermal/MR	[71]
BiNS-Fe@Fe	Laser (808 nm)	PDT/PTT/CDT	HepG-2 [h)] cells	HepG-2 tumor-bearing mice	Optical/Photothermal/ Photoacoustic/MR/CT	[83]
UCNPs@MOFs	Laser (980 nm)	PDT/Chemotherapy/ Immunotherapy	CT26 cells	CT26 tumor-bearing mice	Optical	[42]
CDTN	Laser (671 nm)	PDT/Chemotherapy/Gene therapy	4T1 cells	4T1 tumor-bearing mice	Optical	[136]

[a)]Human head and neck cancer cells; [b)]human epidermoid cancer cells; [c)]mouse breast cancer cells; [d)]human non-small cell lung cancer cells; [e)]mouse liver cancer cells; [f)]mouse colon cancer cells; [g)]human clear cell renal cell carcinoma cells; [h)]human hepatoma cells.

synergistic effect of PDT and chemotherapy, the NCP@pyrolipid nanoparticles exhibited superior antitumor effect (both in tumor volume and weight) for human head and neck cancer SQ20B xenograft mice compared to monotherapy (Fig. 6g and h). In the study of Chen et al., an antitumor drug paclitaxel (PTX) was utilized to induce the self-assembly of Ce6 photosensitizer-modified human serum albumin (HSA) and acyclic Arg-Gly-Asp (cRGDyK) peptide-modified HSA [217]. The self-assembled nanoparticle was composed of a Ce6/PTX-HSA core and a RGD/PTX-HSA shell. Both *in vitro* and *in vivo* studies proved that the Ce6/PTX-HSA@RGD/PTX-HAS nanoparticles could not only target $\alpha v\beta 3$-integrin, but also realize PDT/chemotherapy combination, which significantly enhanced the therapeutic efficacy for cancer.

Chemotherapeutic drugs can be loaded into core–shell structured nanoparticles together with traditional small molecule photosensitizers for combined therapy of PDT/chemotherapy. For example, Wang et al. assembled the ZnPc photosensitizer and DOX on the surface of UCNPs@mSiO_2-CuS nanoparticles for PDT and chemotherapy functions, respectively [208]. Benefiting from the synergistic effect of PDT and chemotherapy, the UCNPs@mSiO_2-CuS-ZnPc-DOX nanoparticles showed superior antitumor efficiencies both *in vitro* and *in vivo*. With the rapid development of photosensitizers, chemotherapeutic drugs are also loaded into core–shell structured nanoparticles that can directly act as photosensitizers. In the study of Yang et al., DOX was loaded into the UCNPs@MIL-100(Fe) nanoparticles for PDT/chemotherapy [218]. The MIL-100(Fe) shell not only served as a photosensitizer to produce ROS under irradiation, but also loaded a large amount of DOX due to its porous structure and high specific area. In order to better regulate their interactions, chemotherapeutic drugs and photosensitizers are placed in different layers independently. Peng et al. prepared the dual-template imprinting polymer nanoparticles for targeted PDT/chemotherapy by encapsulating gadolinium-doped silicon quantum dots and Ce6 photosensitizer in fluorescent SiO_2($FSiO_2$) core and loading DOX and epitope into 3-methacryloxypropyltrimethoxysilane (MPS) shell [219]. Under 655 nm laser irradiation, the implanted Ce6 photosensitizer generated $^1O_2$ to kill cancer cells, combining with the embedded DOX to achieve a synergistic treatment.

Notably, the controllable release of drugs in core–shell structured nanoparticles is critical to obtain a desirable therapeutic efficacy [220,221]. Since tumor microenvironment presents slight acidity, some pH-responsive core–shell structured nanoparticles have been designed to precisely control the release of drugs in tumors [74,188]. For example, Cai et al. constructed pH-responsive α-$NaYbF_4$:Tm@CaF_2:Nd@ZnO (UZNPs)-polyacrylic acid (PAA)-DOX nanoparticles for PDT/chemotherapy (Fig. 7a) [84]. Upon 808 nm NIR laser excitation, the nanoparticles were induced to generate electron-hole pairs, which subsequently reacted with O_2 and H_2O to produce $\cdot O_2^-$ and ·OH respectively for cancer therapy

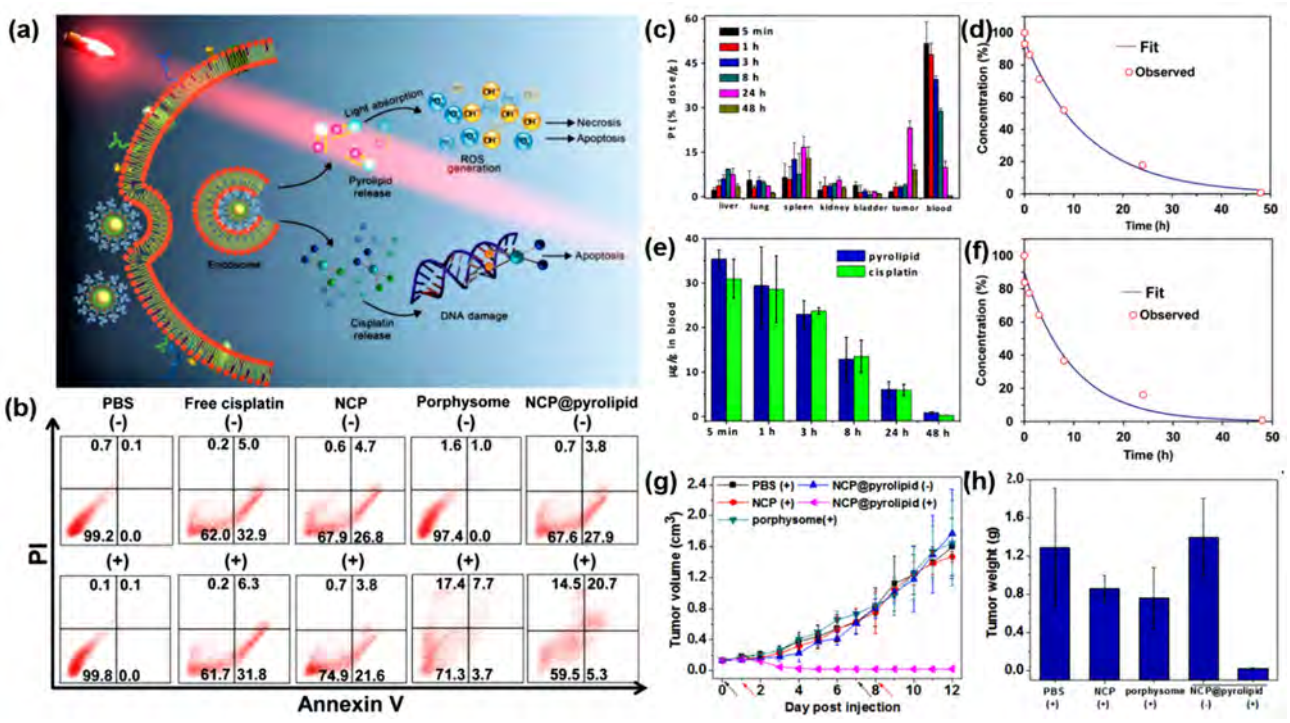

Fig. 6. (a) Proposed cytotoxicity mechanism of the NCP@pyrolipid nanoparticles. (b) Flow cytometry showing the apoptosis and necrosis induced by the NCP@pyrolipid nanoparticles upon irradiation. (c) Tissue distributions of Pt at different time points after intravenous injection of the NCP@pyrolipid nanoparticles. (d) Observed and fitted time-dependent Pt concentrations in blood following the NCP@pyrolipid administration by one-compartment model. (e) Time-dependent pyrolipid and cisplatin concentrations in blood after intravenous injection of the NCP@pyrolipid nanoparticles. (f) Observed and fitted time-dependent pyrolipid concentrations in blood following the NCP@pyrolipid administration by one-compartment model. (g) Tumor growth inhibition curves. (h) Weights of excised tumors on Day 12. Reproduced with permission. [201] Copyright 2015, American Chemical Society.

(Fig. 7b). As shown in Fig. 7c, the electron paramagnetic resonance tests also confirmed the ROS generation. Moreover, the PAA coating could load abundant DOX and decompose at mild acidic tumor microenvironment to release DOX (Fig. 7d). At acid buffer dispersion with pH of 5.5, the nanoparticles released about 82% of DOX in the first 8 h, verifying the superior pH-activable ability (Fig. 7e). In addition to pH-responsive core–shell structured nanoparticles, some ROS-responsive core–shell structured nanoparticles have also been developed to regulate the release of drugs due to the large number of ROS generated during PDT. In the study of Lee et al., a chitosan shell was coated on a ROS-generating PhA-linked poly(hydroxyethyl methacrylate) (poly-HEMA) core, and then linked to an anticancer drug 5′-deoxy-5-fluorocytidine (DFCR) through phenylboronic acid to form a ROS cleavable boronic ester for PDT/chemotherapy [222]. Sun et al. fabricated a ROS-reponsive nanoparticle composed of a single thioether-bridged paclitaxel (PTX)-oleic acid (OA) prodrug (PTX-S-OA) core and a pyropheophorbide a (PPa)-polyethylene glycol 2000 (PEG_{2k}) shell for PDT/chemotherapy [128]. Under laser irradiation, the ROS generated by PPa-PEG_{2k} shell not only were used for PDT, but also promoted the release of PTX from PTX-S-OA in combination with endogenous ROS.

4.2. PDT combined with photothermal therapy

Photothermal therapy (PTT) is a promising noninvasive cancer treatment method that exploits the NIR light and photothermal agents to convert light energy to heat energy, which can effectively destroy tumor tissues and cells [223–225]. Because of the similar photoactivation conditions to PDT and the ability to overcome imperfections of PDT, PTT has been extensively employed to combine with PDT to maximize the curative effect for cancer [204,226,227]. In this synergistic therapeutic modality, the appropriate photothermal effect can increase the permeability of cell membranes, thereby promoting the efficient absorption and penetration of tumor cells to nanoparticles. Meanwhile, it can also accelerate the blood flow velocity in tumor and hence transport more O_2 to attenuate the tumor hypoxia. Recently, a series of NIR light absorbing nanomaterials have been applied to construct core–shell structured nanoparticles for combined therapy of PDT/PTT, such as gold nanostructures (e.g., nanorods [202,228] and nanocages [229,230]), PDA [66,71,231], Nd^{3+}-doped UCNPs [232,233], black TiO_2 [166,203] and copper sulfide [208,234,235].

Among them, gold nanostructures are considered to have great potential in PDT/PTT owing to their SPR induced excellent photothermal effect [236–238]. For example, Qin et al. coated the AuNR with a HB photosensitizer-incorporated $mSiO_2$ shell and a folate-modified lipid (LF) bilayer for PDT/PTT [57]. The AuNR@$mSiO_2$-HB@LF nanoparticles possessed a strong SPR peak at 801 nm, which was expected to achieve PTT under NIR light irradiation. After being irradiated by a 808 nm laser (1.5 W cm^{-2}) for 5 min, the temperature of AuNR@$mSiO_2$-HB@LF suspension (0.1 mg mL^{-1}) increased by about 50 °C, which was enough to kill the tumor cells. Moreover, the yield of photoinduced ROS was enhanced by hyperthermia. Therefore, the AuNR@$mSiO_2$-HB@LF nanoparticles could significantly eliminate the MCF-7 tumor in BALB/c nude mice because of the synergistic effect of PDT and PTT. To improve the photothermal conversion efficiency and photothermal stability of gold nanostructures, Zhang et al. synthesized gold cube-in-cubes for developing the CCmMC PDT/PTT agent [190]. The CCmMC nanovehicles were constructed by loading Mn-Cdots on gold cube-in-cubes@$mSiO_2$ core–shell structured nanoparticles (Fig. 8a). As displayed in Fig. 8b-d, the temperature of CCmMC suspension increased as the increase of CCmMC

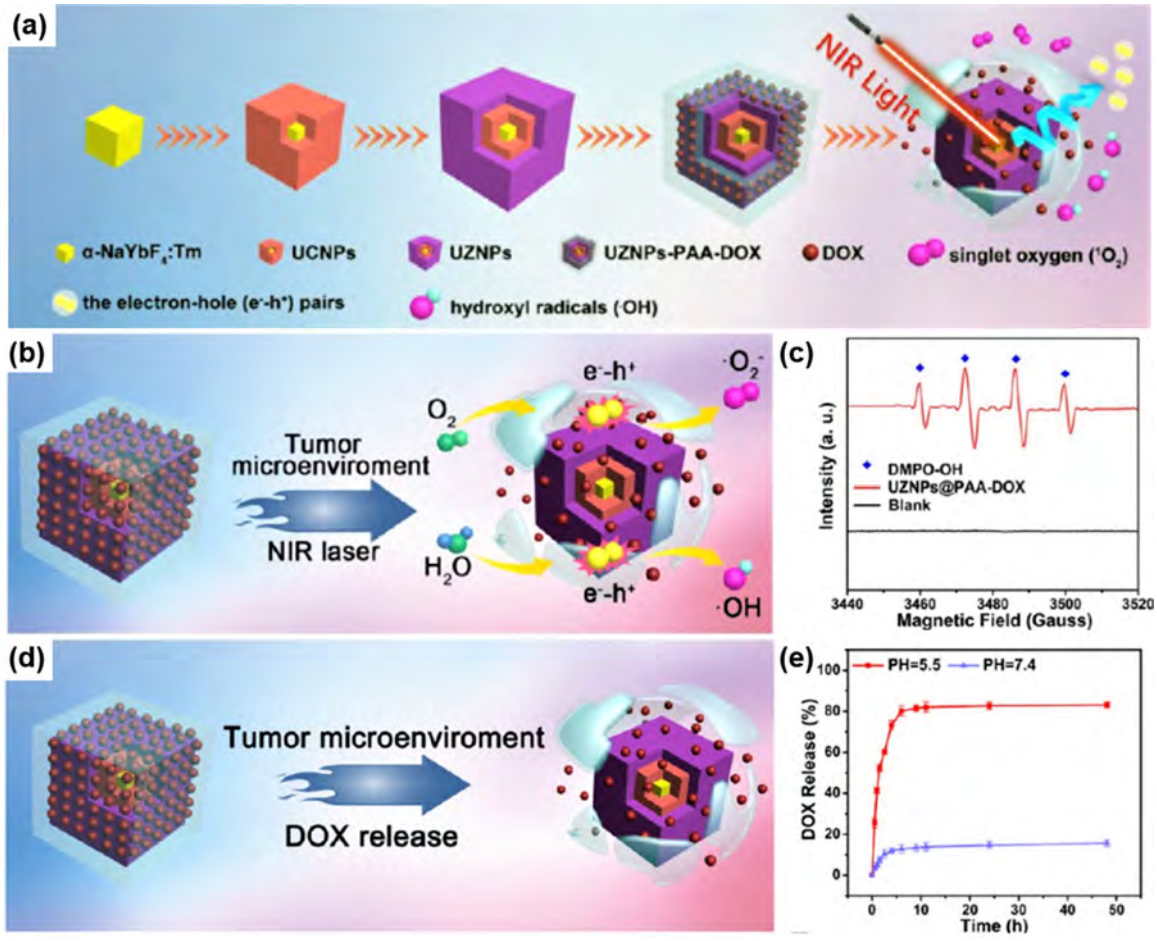

Fig. 7. (a) Schematic illustration for the preparation of UZNPs-PAA-DOX nanoparticles. (b) Mechanism of 808 nm NIR laser irradiation-triggered PDT over the UZNPs-PAA-DOX nanoparticles. (c) Electron paramagnetic resonance spectra of the UZNPs-PAA-DOX nanoparticles. (d) Schematic illustration for the pH-responsive drug release of UZNPs-PAA-DOX nanoparticles. (e) DOX release profile of the UZNPs-PAA-DOX nanoparticles in PBS with different pH values. Reproduced with permission. [84] Copyright 2020, American Chemical Society.

concentration and irradiation power density, implying the high NIR light-induced photothermal effect of CCmMC. Fig. 8e and f further demonstrated that the CCmMC possessed a superior photothermal conversion efficiency of 65.6% and excellent photothermal stability upon 808 nm laser excitation. After coupling with the Mn-Cdots-induced favorable PDT effect, the CCmMC exhibited desirable therapy efficacy in treating 4 T1 tumor xenografts on nude mice under the dual laser (635 and 808 nm) irradiation.

PDA has also been widely employed as a PTT agent in combined therapy of PDT/PTT due to its pronounced absorption in NIR region, satisfactory photothermal conversion capacity and outstanding biocompatibility [239,240]. In the study of Cen et al., a PDA shell was coated on the methylene blue (MB)-loaded UCNPs@SiO_2 nanoparticles for PDT/PTT [241]. The temperature of UCNPs@SiO_2-MB@PDA suspension (0.2 mg mL^{-1}) rose to 52.2 °C after 10 min of 980 nm laser (1.5 W cm^{-2}) irradiation, indicating its great photothermal conversion ability. Through the FRET from UCNPs to MB photosensitizer and PDA, the UCNP@SiO_2-MB@PDA nanoparticles presented excellent PDT/PTT synergistic effect for killing the cancer cells under 980 nm laser irradiation. Yang et al. utilized PDA core as the template to prepare lactose acid (LA)-grafted PDA@cobalt phytate (CoPA) nanoparticles for PDT/PTT [242]. Benefiting from the PDA-endowed PTT effect, CoPA-induced PDT effect and LA-endued targeting capability, the PDA@CoPA-LA nanoparticles exhibited superior antitumor performances both *in vitro* and *in vivo*. Moreover, the abundant amino and catechol groups on the surface of PDA make it easy to be modified by various functional biomolecules [243]. Zeng et al. improved the performance of targeted breast cancer treatment in PDT/PTT by introducing FA molecules on the surface of MnO_2-Ce6@PDA nanoparticles [126].

In addition to the combinational therapeutic modality of PDT/chemotherapy and PDT/PTT summarized above, tri-modal PDT/PTT/chemotherapy has been developed to further lower laser power and reduce drug dosage in cancer treatment. For example, Zeng et al. employed AuNR as the seed crystal to prepare AuNR@MOFs@camptothecin (CPT) nanoparticles for PDT/PTT/chemotherapy (Fig. 9a-e) [73]. As shown in the *in vivo* photothermal images (Fig. 9f), the temperature of AuNR@MOFs@CPT nanoparticles-injected tumor increased quickly from 28.5 to 48.4 °C after 2 min of 808 nm laser irradiation, and then reached a steady temperature of 54.8 ± 1.2 °C, which was sufficient to cause the death of cancer cells. Meanwhile, the photothermal effect of AuNR could also accelerate the intracellular release of CPT (Fig. 9g and h). By virtue of the synergistic effect of photoinduced ROS, photothermal effect and released CPT, the combined therapy significantly raised the survival rate of 4 T1 tumor-bearing mice (Fig. 9i). Furthermore, the AuNR@MOFs@CPT nanoparticles restrained the hepatic metastases because of its accumulation in liver and tumor position (Fig. 9j and k). And after 50 d of treatment of mice with AuNR@MOFs@CPT nanoparticles, the tumors almost completely disappeared (Fig. 9l). Additionally, Chen et al. designed ROS-responsive PPID nanoparticles which was composed by

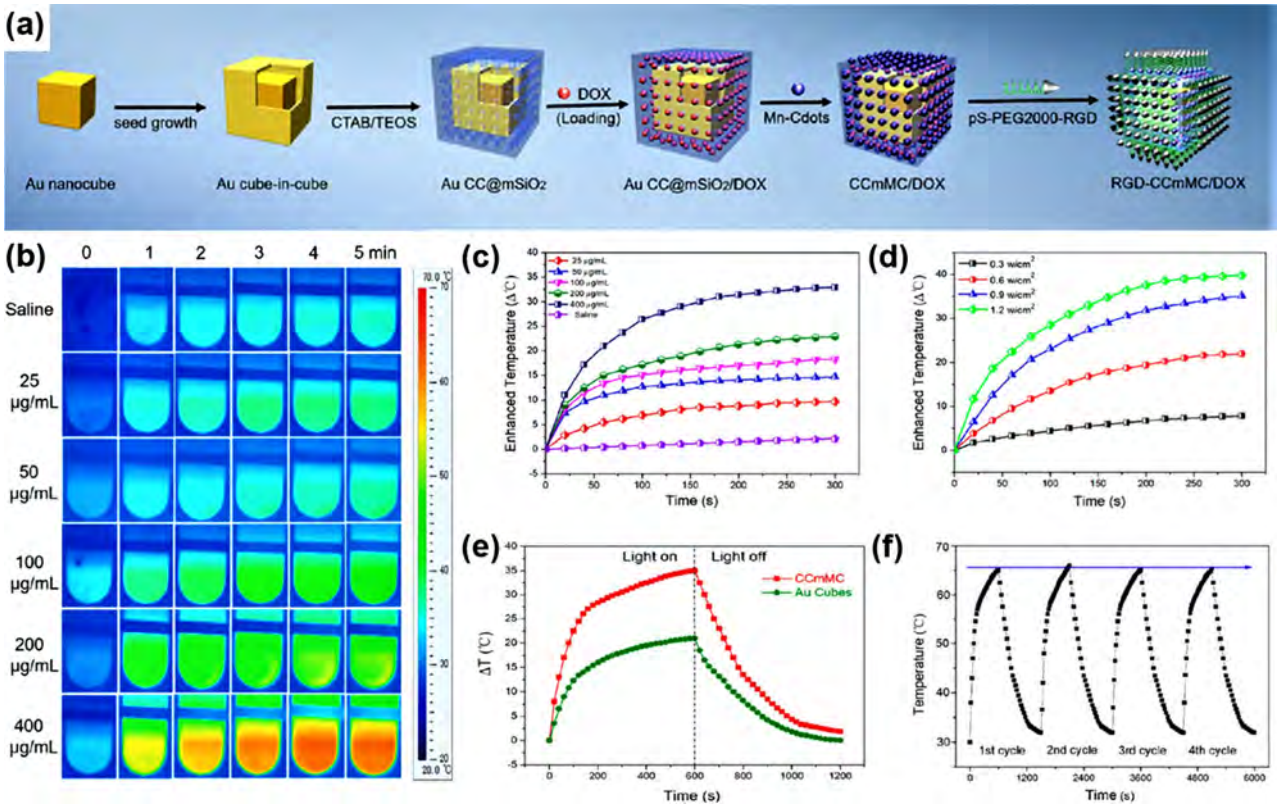

Fig. 8. (a) Schematic illustration for the preparation of RGD-CCmMC/DOX nanoparticles. (b) Thermographic images of the CCmMC aqueous solutions irradiated with 808 nm laser at a power intensity of 1 W cm^{-2}. (c) Photothermal conversion characterizations of the CCmMC aqueous solution of various concentrations under 1 W cm^{-2} 808 nm laser irradiation. (d) Temperature elevation profiles of the CCmMC solutions under various laser power densities. (e) Temperature changes in CCmMC and Au Cube aqueous solutions in response to NIR laser on and off. (f) Temperature curves of CCmMC under continuous NIR laser irradiation for 4 cycles. Reproduced with permission. [190] Copyright 2019, American Chemical Society.

self-assembly of a IR780 photosensitizer and DOX co-loaded poly (β-amino ester) core and a propylene glycol alginate sodium sulfate shell for PDT/PTT/chemotherapy [244]. The PPID nanoparticles could greatly improve the PDT and PTT performances of IR780 *in vitro* and further promote the internalization of IR780 and DOX in Hep1-6 cells. Compared with free IR780 and free DOX, the PPID nanoparticles showed synergistic cytotoxicity in Hep1-6 cells under 808 nm laser irradiation.

4.3. PDT combined with immunotherapy

PDT can not only kill tumor cells directly, but also induce immunogenic cell death (ICD) of tumor cells, thereby promoting the maturation of dendritic cells and activation of effector cells, and ultimately leading to a systemic antitumor immune response [245–247]. Recent studies have reported that some core–shell structured nanoparticles can evoke an antitumor immune response during the process of PDT to enhance the therapeutic efficacy for cancer [206,230]. For example, in the study of Liang et al., in addition to efficiently destroying 4 T1 breast cancer cells, the abundant ROS generated by gold nanocage@MnO_2 nanoparticles under laser irradiation also triggered the ICD-mediated antitumor immune response [229]. Specifically, the dying cancer cells released damage associated molecular patterns (e.g., calreticulin, adenosine triphosphate and high mobility group protein B1) for the dendritic cells maturation. And then the specific effector cells (e.g., $CD4^+$ T cells, $CD8^+$ T cells and NK cells) were activated to prevent the tumor growth and metastasis. Unfortunately, the immune response induced by PDT is usually mild and not enough to completely suppress the tumor metastasis. Immunosuppressive tumor microenvironment may significantly depress the PDT-induced immunotherapy efficacy through the immune checkpoint pathway [198,248].

As an effective cancer treatment method with low side effects, immunotherapy kills tumor cells by activating the body's own immune system [249]. Among them, checkpoint blockade immunotherapy has attracted much attention, which exploits inhibitor molecules to target the regulatory pathways in T cells for modulating immunosuppressive tumor microenvironment and enhancing antitumor immune response [250,251]. Especially, the programmed death 1/programmed death ligand 1 (PD-1/PD-L1) blockade has already been approved by the U.S. Food and Drug Administration (FDA) to treat diverse tumors [252,253]. Although checkpoint blockade immunotherapy has achieved clinical success, it is only effective in tumors pre-infiltrated by T cells. Accordingly, PDT that can induce ICD of tumor cells may improve its efficacy. In this case, the combined therapy of PDT/immunotherapy based on core–shell structured nanoparticles has the potential to promote the primary tumors destruction and distant metastatic tumors control [254]. In the study of Duan et al., the Zn-pyrophosphate (ZnP)@pyrolipid nanoparticles (Fig. 10a) were fabricated to combine PDT with checkpoint blockade immunotherapy for the treatment of metastatic breast cancer [205]. As depicted in Fig. 10b, the combination of ZnP@pyrolipid-mediated PDT with PD-L1 antibody (α-PD-L1)-mediated immunotherapy not only destroyed the primary tumors but also remarkably inhibited the metastasis to lung in a 4 T1 mTNBC murine model. Compared to the PBS control group, the ZnP@pyrolipid-mediated PDT reduced the 4 T1 tumor by 68% in volume and 75% in weight. But after the introduction of α-PD-L1, the 4 T1 tumor was completely eradicated. Moreover,

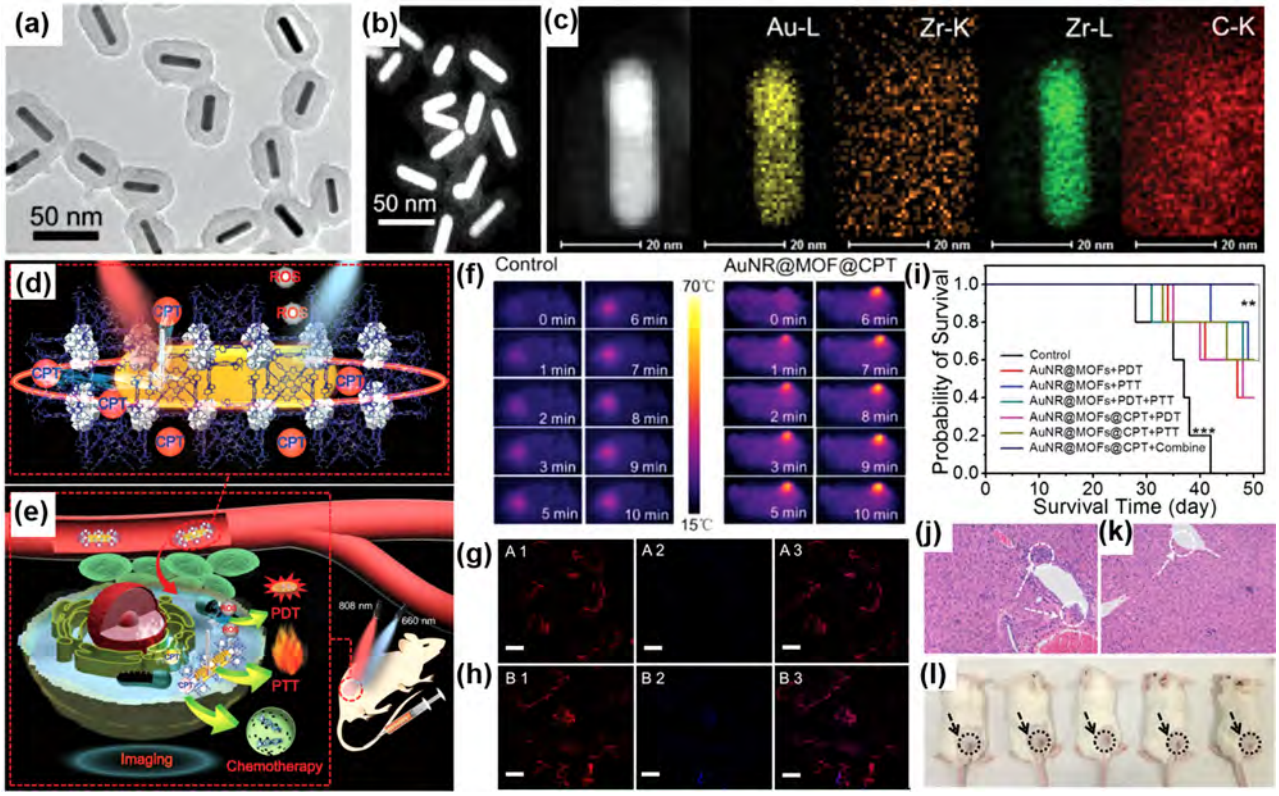

Fig. 9. (a) TEM image, (b) STEM-HAADF image and (c) EDX elemental mapping images of the AuNR@MOFs nanoparticles. (d) The structure of AuNR@MOFs@CPT nanoparticles. (e) The combined PDT/PTT/chemotherapy of tumor. (f) The *in vivo* thermal images of the mice after intravenous injection of PBS and AuNR@MOFs@CPT with 808 nm laser irradiation. (g) The intracellular drug release behavior of AuNR@MOFs@CPT in dark and (h) under 808 nm laser irradiation. (i) Survival curves of tumor-bearing mice after different treatments (n = 5, $^{**}p < 0.01$ and $^{***}p < 0.01$ were calculated by a Student's t test). (j) H&E staining of liver after intravenous injection of PBS and (k) AuNR@MOFs@CPT on day 18. (l) The photograph of tumor-bearing mice treated with AuNR@MOFs@CPT for combined therapy after 50 d. Reproduced with permission. [73] Copyright 2017, Wiley-VCH.

the results of gross examination of lung tumor nodules demonstrated that the combined therapy was much more effective than ZnP@pyrolipid-mediated PDT or α-PD-L1-mediated immunotherapy alone in restraining lung metastasis.

To further enhance the therapeutic efficacy for cancer, tri-modal therapeutic approach has been developed on the core–shell structured nanoparticles, such as PDT/chemotherapy/immunotherapy [42,255] and PDT/PTT/immunotherapy [71]. As shown in Fig. 11a, Shao et al. constructed tirapazamine (TPZ)-encapsulated UCSs nanoparticles to combine PDT/chemotherapy with checkpoint blockade immunotherapy for the treatment of hypoxic tumors [42]. The combined therapy effectively inhibited the growth of primary tumors and distant tumors in CT26 tumor-bearing mice both in tumor volume and weight. Meanwhile, in the combined therapy group, the percentages of infiltrating $CD45^+$ cells, $CD4^+$ T cells, $CD8^+$ T cells and B cells were increased in both primary tumors and distant tumors (Fig. 11b-e), indicating that the combination of TPZ/UCSs-mediated PDT/chemotherapy with α-PD-L1-mediated immunotherapy improved the immunotherapeutic efficacy through the infiltration of effector T cells. Besides, in the study of Yan et al., PDA@UCNPs-PEG/Ce6 nanoparticles were assembled to combine PDT/PTT with α-PD-L1-mediated immunotherapy for inhibiting the tumor metastasis and relapse [71]. In the combined therapy group, most of the 4 T1 tumor-bearing mice could survive 100 days, and the survival rate was almost as high as 77.8%, which was much higher than that of the control groups.

4.4. PDT combined with other therapies

In addition to chemotherapy, PTT and immunotherapy, PDT can also be combined with other therapies, such as radiotherapy [256,257], gene therapy [258,259] and chemodynamic therapy [260,261], to enhance the therapeutic efficacy. With the development of nanotechnology, some core–shell structured nanoparticles have been designed to combine PDT with these therapies. Radiotherapy is a conventional cancer treatment method, which utilizes ionizing radiation to control or kill tumor cells and is not limited by the tissue penetration depth [262]. Benefiting from the inherent antitumor efficacy and strong penetration ability of ionizing radiation, the combined therapy of PDT/radiotherapy that employs a single excitation source will present a great clinical significance [263]. In the study of Zhang et al., $LiYF_4$:Ce@SiO_2@ZnO nanoparticles were fabricated for synchronous PDT and radiotherapy under X-ray radiation [153]. The growth of tumor treated by PDT/radiotherapy was almost completely suppressed after 15 days, while the growth of tumor treated by radiotherapy alone was only slightly inhibited, implying the excellent synergistic effect of PDT and radiotherapy.

Gene therapy is a promising cancer treatment method, which delivers therapeutic nucleic acids into the tumor cells to correct or compensate cancers caused by genetic defects and anomalies [264]. Among various therapeutic nucleic acids, small interfering RNAs (siRNAs) that can intracellularly silence disease-causing genes have attracted tremendous interest since they can remarkably improve the specificity and efficacy of gene therapy [265,266]. Nevertheless, the cellular impermeability and easy degradability of siRNAs hinder their transfer into tumor cells. A recent study suggested that the core–shell structured photodynamic nanoparticle is an excellent carrier that can simultaneously deliver chemotherapeutic drugs and siRNAs into tumor cells for photodynamic synergistic therapy [136]. As shown in Fig. 12a, core–shell structured nanoparticles named

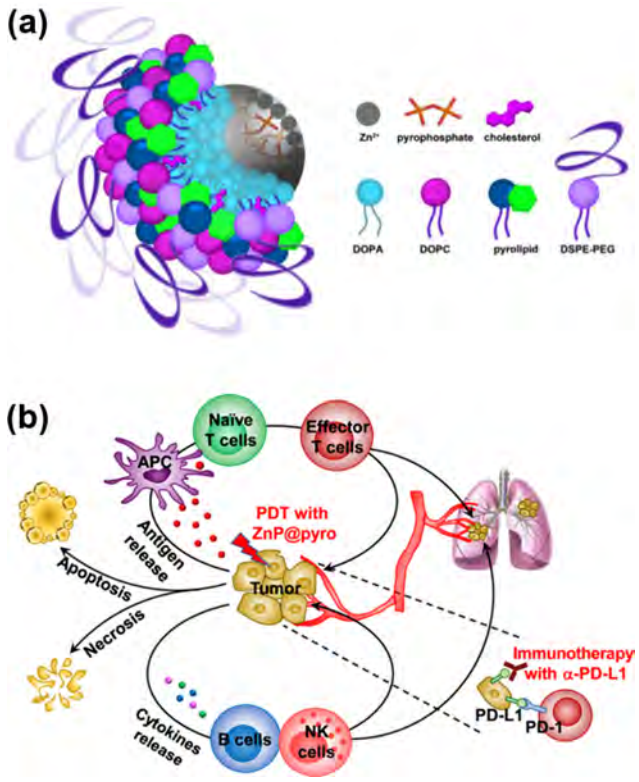

Fig. 10. (a) Scheme showing the Zn-pyrophosphate core and the asymmetric lipid bilayer shell of ZnP@pyrolipid nanoparticles. (b) Immunogenic ZnP@pyrolipid PDT sensitizes tumors to PD-L1 blockade immunotherapy for the treatment of metastatic tumors. Reproduced with permission. [205] Copyright 2016, American Chemical Society.

CDTNs were designed via self-assembly of 1,2-distearoyl-*sn*-glycero-3-phosphoethanolamine-*N*-[maleimide-(polyethylene glycol)$_{5000}$ (DSPE-PEG), poly-β-aminoester derivative Ce6-grafted poly [(1,4-butanediol)-diacrylate-β-oligoethylenimine$_{600}$] (Ce6-PDOEI), docetaxel and anti-Twist siRNA for tri-modal PDT/chemotherapy/-gene therapy of metastatic triple-negative breast cancer (mTNBC). In the superficial part of the tumor, CDTNs eliminated the primary tumor and inhibited its pulmonary metastasis mainly through PDT. While in the deep part of the tumor, CDTNs eliminated the primary tumor mainly through PDT-potentiated chemotherapy and inhibited its pulmonary metastasis through PDT-potentiated gene therapy and chemotherapy (Fig. 12b). Therefore, compared with the monotherapy and dual-modal therapy, the CDTNs exhibited superior efficacy in inhibiting the growth of the primary tumor and its pulmonary metastasis (Fig. 12c-f).

Chemodynamic therapy (CDT) is a novel cancer treatment method, which exploits transition metals and weak acidic TME to catalyze overexpressed endogenous H_2O_2 to produce ·OH for killing cancer cells [267,268]. Since O_2 and ·OH can be generated during CDT through Fenton/Fenton-like reactions, the tumor hypoxia will be alleviated and the therapeutic efficacy of PDT will be enhanced [269,270]. Accordingly, core–shell structured nanoparticles have been employed to combine PDT with CDT for synergistic therapy more recently. As depicted in Fig. 13a, Xu et al. constructed PEG-modified lanthanide-doped nanoparticles@copper/manganese silicate nanospheres (PEG/LDNPs@CMSNs) for PDT/CDT synergistic therapy [207]. The CMSNs alleviated tumor hypoxia by decomposing H_2O_2 to generate O_2, and served as photosensitizers to utilize the O_2 to generate $^1O_2$ upon NIR laser excitation for PDT. Meanwhile, the tumor glutathione (GSH)-triggered release of Fenton-like Mn^{2+} and Cu^+ ions led to CDT by inducing the generation of ·OH (Fig. 13b). Benefiting from the synergistic effect of PDT and CDT, the PEG/LDNPs@CMSNs displayed superior antitumor effects both *in vitro* and *in vivo* under 980 nm NIR laser irradiation (Fig. 13c and d). Moreover, in the study of Qi et al., $NaGdF_4$:Er,Yb@$NaGdF_4$:Nd@Cu(II) boron-imidazolate frameworks (CSNPs@Cu-BIF) nanoparticles were assembled for PDT/PTT/CDT synergistic therapy [233]. Upon 808 nm NIR laser excitation, the nanoparticles exhibited enhanced antitumor efficacy for *in vitro* MCF-7 cancer cells and *in vivo* MCF-7 tumor-bearing nude mice.

5. Core-shell structured nanoparticles for imaging in PDT-based cancer treatment

Molecular imaging techniques play a vital role in diagnosis and treatment of cancer. In recent years, a variety of molecular imaging techniques, such as optical imaging, photothermal imaging,

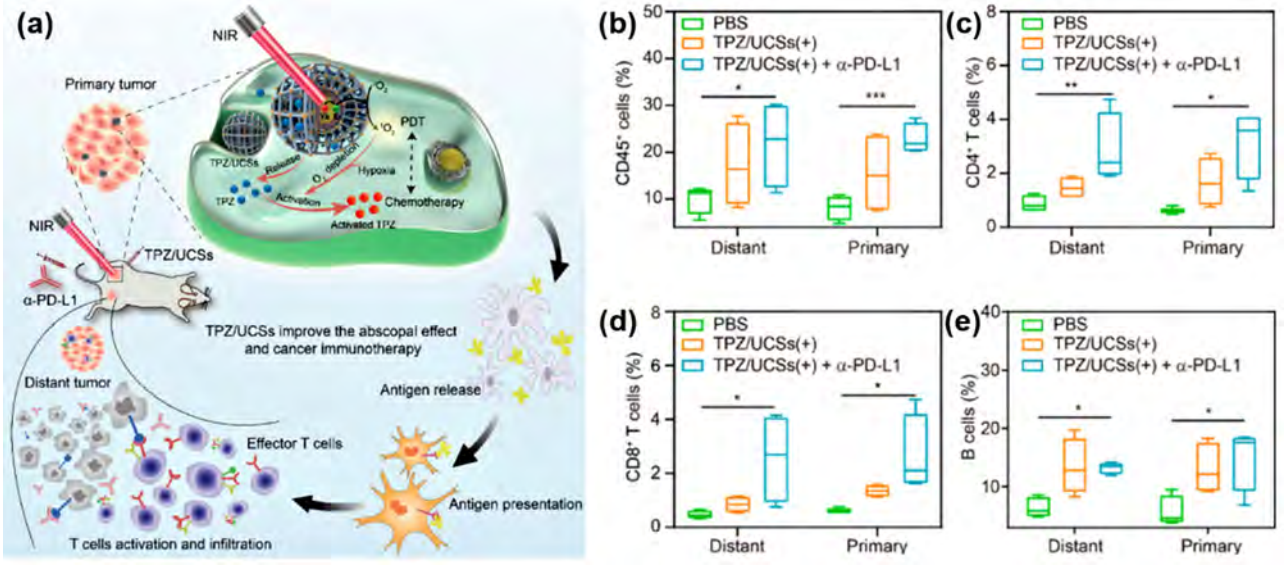

Fig. 11. (a) Schematic illustration of the structure of TPZ/UCSs nanoparticles and their application to tumor treatment through a combination of NIR light-triggered PDT and hypoxia-activated chemotherapy with immunotherapy. Percentage of tumor-infiltrating (b) $CD45^+$ cells, (c) $CD4^+$ T cells, (d) $CD8^+$ T cells and (e) B cells in total tumor cells. Data are means ± SD, $n = 4$. $^*p < 0.05$, $^{**}p < 0.01$ and $^{***}p < 0.001$. Reproduced with permission. [42] Copyright 2020, American Chemical Society.

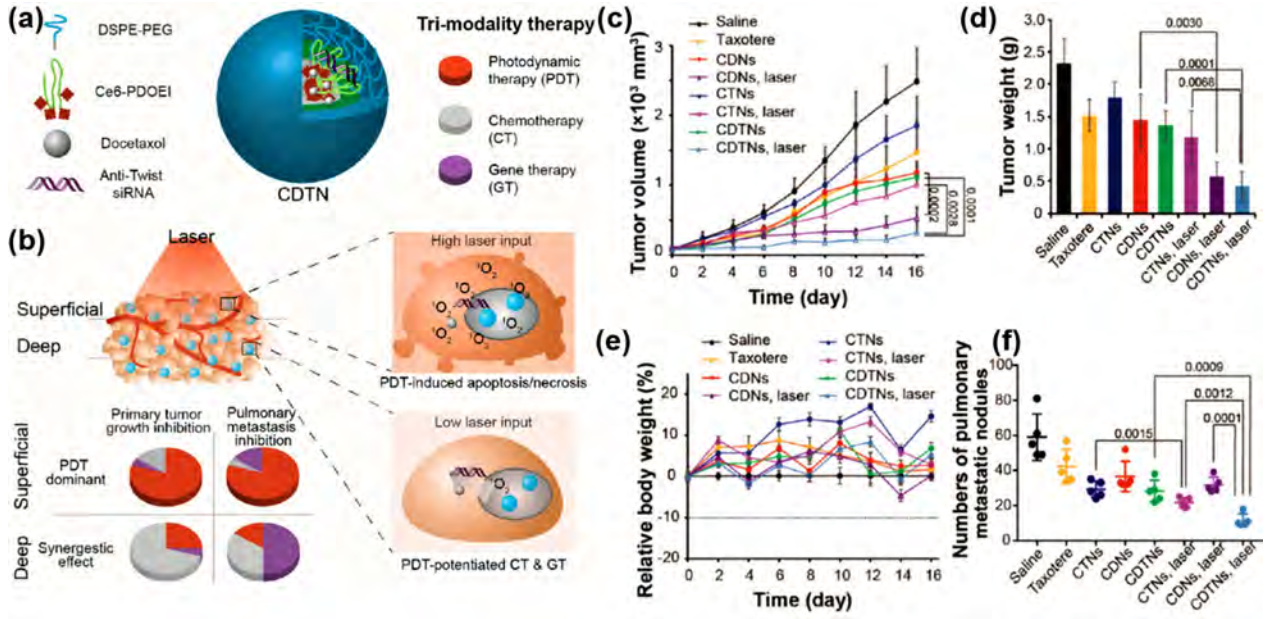

Fig. 12. (a) Schematic illustration of design and function of CDTNs. (b) Depth-dependent mechanism of CDTNs against mTNBC. (c) Growth profiles and (d) weights of primary TNBC tumors in mice receiving different treatments. (e) Changes in body weights of 4T1-bearing mice. (f) Comparison of pulmonary metastatic nodules of 4T1 tumor-bearing mice treated with various treatments. Reproduced with permission. [136] Copyright 2018, American Chemical Society.

photoacoustic imaging, magnetic resonance imaging and computed tomography imaging have been employed for the imaging in PDT-based cancer treatment [271–273]. Notably, core–shell structured nanoparticles are widely used in the PDT-based cancer treatment, and can be used as effective contrast agents for the imaging in PDT-based cancer treatment. Compared with single-component nanoparticles, core–shell structured nanoparticles present unique imaging behavior as they possess combinatorial characteristics of both core and shell materials, which is conductive to multimodal imaging [121,200,274].

5.1. Optical imaging

Optical imaging is a noninvasive and safe imaging strategy, which utilizes the inherent luminescent property of the nanomaterials [275,276]. Some photosensitizers in the excited state not only produce cytotoxic ROS, but also emit luminescence when they back to the ground state [277]. Consequently, in addition to being employed for PDT, these photosensitizers can also be utilized for the optical imaging in PDT-based cancer treatment. In recent years, various small molecule photosensitizers, such as PhA [278,279], Ce6 [97,103] and ICG [68,78], have been encapsulated into core–shell structured nanoparticles for fluorescence imaging-guided PDT. In the study of Liu et al., the biodistribution of RC@TFC nanoparticles in mice bearing subcutaneous MDA-MB-231 tumors could be easily tracked through an ex vivo imaging system because of the intrinsic fluorescence of Ce6 [129]. The results of fluorescent imaging displayed that both free Ce6 and RC@TFC nanoparticles were extensively distributed throughout the mouse after 1 h of injection (Fig. 14a). After 24 h, most of the free Ce6 was cleared from the mouse, while the RC@TFC nanoparticles accumulated in the tumor site and showed strong fluorescence, which might be ascribed to the EPR effect (Fig. 14b). Similarly, loading ICG photosensitizer through electrostatic adsorption on the gold nanocage@MnO_2-hyaluronic acid nanoparticles to realize the fluorescence emission for fluorescence imaging-guided PDT was reported by He et al. [230] In addition, quantum dots (QDs) are utilized for fluorescence imaging, but they are limited by the low water solubility and tendency to photooxidation [280]. Core-shell structured photodynamic nanoparticles can efficiently encapsulate the QDs to minimize these limitations. Hence these core–shell structured nanoparticles possessed excellent ability for the fluorescence imaging in PDT-based cancer treatment [108,190,219].

Benefiting from the exceptional photophysical properties, UCNPs also present good fluorescence imaging ability [281]. After coating them with suitable materials and photosensitizers, these core–shell structured nanoparticles can be applied in the fluorescence imaging-guided PDT. Wang et al. prepared UCNPs@SiO_2(MB)@mSiO_2(RhB)-β-cyclodextrin nanoparticles for simultaneous fluorescence imaging, PDT and drug delivery [282]. Upon 980 nm NIR laser excitation, the UCNPs core emitted 540 nm green light for fluorescence imaging and 660 nm red light to activate photosensitizers for $^1O_2$ generation. In the study of Tang et al., a mSiO_2 shell was decorated on UCNPs and then the ZnPc photosensitizer was incorporated into the mSiO_2 shell to construct a fluorescence imaging-guided PDT theranostic nanoplatform [56]. In this nanoplatform, the green emission excited by the 808 nm NIR laser was used for real-time imaging, while the red emission excited by the 980 nm NIR laser was used to produce ROS for PDT (Fig. 14c). Furthermore, compared with the traditional fluorescence imaging in the first NIR window (NIR-I, 700–900 nm), recently developed fluorescence imaging in the second NIR window (NIR-II, 1000–1700 nm) possess deeper tissue penetration ability, better spatial resolution and higher signal-background-ratio [283–285]. For example, Wang et al. fabricated UCNPs@mSiO_2(Ce6, atovaquone)@MnO_2 nanoparticles for NIR-II fluorescence imaging-guided PDT [286]. Upon 808 nm NIR laser excitation, the nanoparticles emitted intense NIR light: 1060 nm (Nd: $^4F_{3/2} \rightarrow {}^4I_{11/2}$), 1350 nm (Nd: $^4F_{3/2} \rightarrow {}^4I_{13/2}$) and 1520 nm ($Er^{3+}$: $^4I_{11/2} \rightarrow {}^4I_{15/2}$), which promoted the NIR-II fluorescence imaging.

5.2. Photothermal imaging

Photothermal imaging is a sensitive imaging strategy based on the difference of temperature, which is often operated in conjunction with PTT [287,288]. The core–shell structured nanoparticles

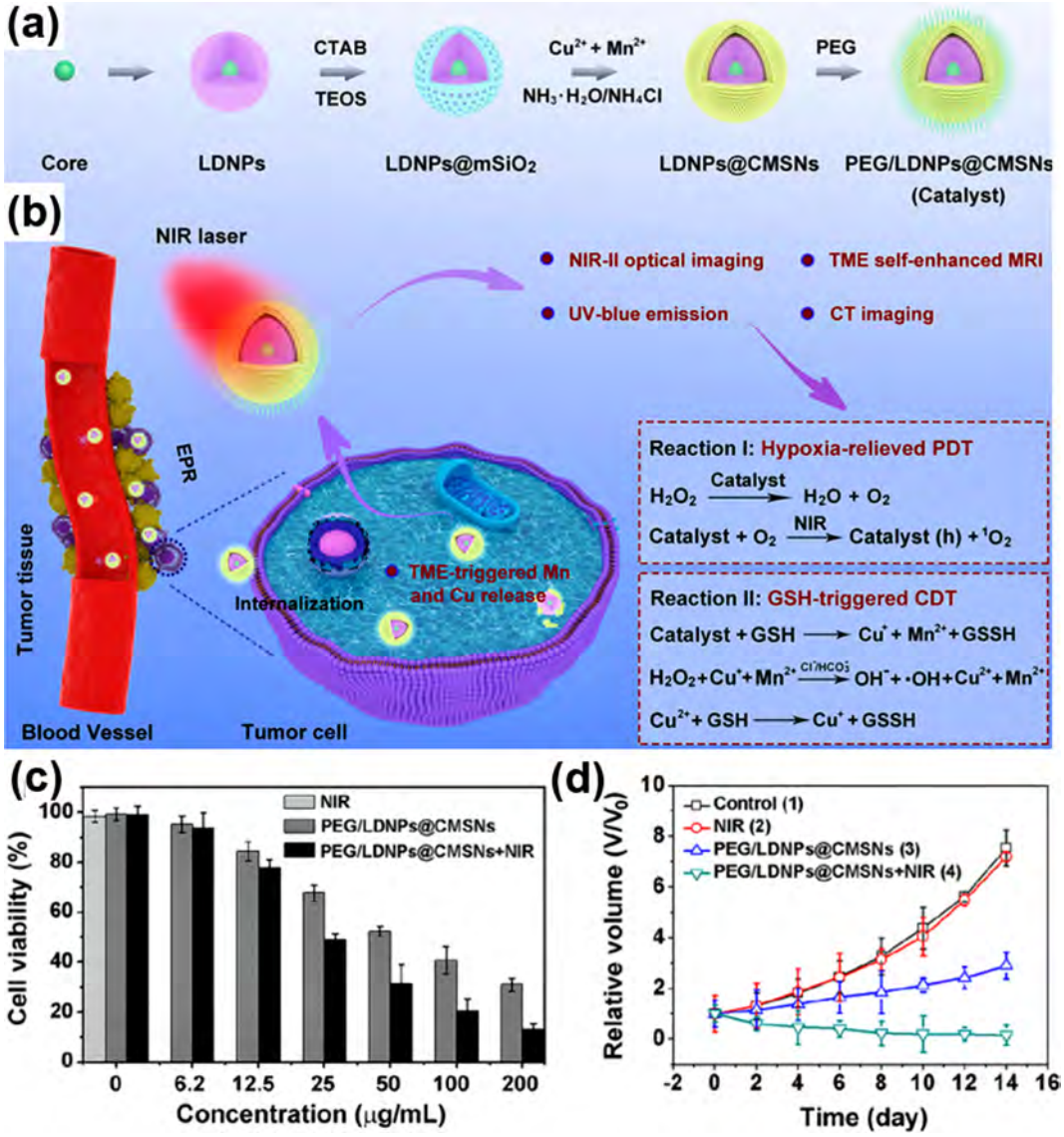

Fig. 13. (a) Schematic illustration of the synthesis of PEG/LDNPs@CMSNs and (b) the theranostic mechanism of PEG/LDNPs@CMSNs for TME and NIR laser co-enabled PDT/CDT and trimodal bioimaging. (c) Viabilities of HeLa cells in the control group and treated with NIR, PEG/LDNPs@CMSNs and PEG/LDNPs@CMSNs plus NIR. (d) Variations in the relative tumor volume achieved from the mice under different treatments. Reproduced with permission. [207] Copyright 2020, American Chemical Society.

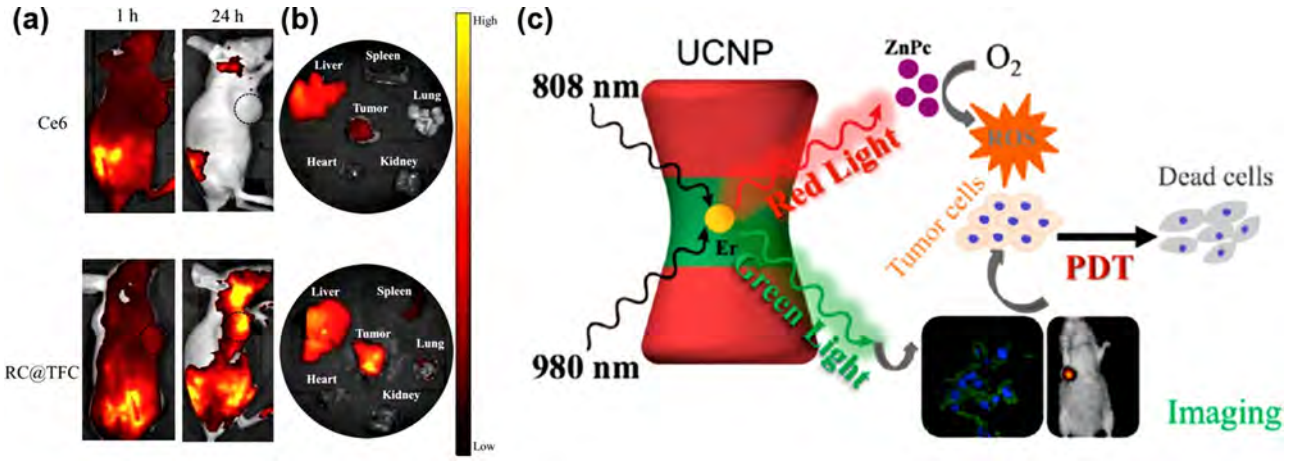

Fig. 14. (a) *In vivo* (1 vs 24 h post injection) and (b) *ex vivo* (24 h post injection) fluorescent imaging of MDA-MB-231 tumor bearing mice treated with free Ce6 and RC@TFC. Reproduced with permission. [129] Copyright 2019, American Chemical Society. (c) Mechanism of the UCNPs@mSiO$_2$(ZnPc) nanoparticles for fluorescence imaging-guided PDT. Reproduced with permission. [56] Copyright 2019, American Chemical Society.

that applied in combined therapy of PDT/PTT has the potential for photothermal imaging. For example, Wang et al. incorporated oxygen vacancy-enriched core–shell structured crystalline@amorphous black TiO_2 into a chitosan matrix for synchronous PDT/PTT and photothermal imaging [166]. As monitored by the photothermal images (Fig. 15a), the temperature of the tumor treated with the BT-CTS thermogels rapidly increased and exceeded 50 °C after being irradiated by a 808 nm laser (0.32 W cm^{-2}) for 15 min. In the study of Ou et al., zinc porphyrin@PDA nanoparticles were synthesized for photothermal imaging-guided PDT/PTT [289]. Photothermal images demonstrated that the temperature of the tumor injected with zinc porphyrin@PDA nanopartciles quickly rose from 35.0 °C to 52.0 °C after 5 min of 660 nm laser (0.75 W cm^{-2}) irradiation, while the temperature of the tumor injected with PBS only increased about 1 °C. Similarly, Huang et al. constructed Cu_{2-x}-S@MnS nanoparticles for photothermal imaging-guided PDT/PTT [61]. The intense optical absorption of the Cu_{2-x}S@MnS nanoparticles in NIR region resulted in the excellent photothermal conversion and photothermal imaging property.

5.3. Photoacoustic imaging

Photoacoustic imaging utilizes the (laser) light pulses to irradiate the sample to generate ultrasound signals for the images creation. It possesses the advantages of both optical and ultrasonic imaging, such as high spatial resolution, high optical contrast and deep penetration [290–292]. Recently, core–shell structured nanoparticles with superior absorption properties in the visible or near-infrared light region have been favored in photoacoustic imaging during PDT-based cancer treatment. For example, Tan et al. monitored the tumor accumulation behavior of ICG-Ag@PANI nanoparticles during the PDT/PTT by photoacoustic imaging due to their strong optical absorbance [68]. Compared with the ICG, PANI and Ag@PANI-treated tumors, the ICG-Ag@PANI-treated tumor exhibited the strongest photoacoustic signals, which was about 7.6- and 2.5-fold that of ICG and Ag@PANI-treated tumors, respectively. Besides, Wang et al. reported that the Au@Rh-ICG nanoparticle coated with tumor cell membrane (CM) could serve as a contrast agent for photoacoustic imaging during PDT due to its strong NIR absorption [78]. As shown in Fig. 15b, after the intravenous injection of Au@Rh-ICG-CM nanoparticles, the photoacoustic signals in the tumor region gradually increased and reached the strongest after 12 h, which was beneficial to trace the tissue distribution of the nanoparticles and guide the treatment process.

5.4. Magnetic resonance imaging

Magnetic resonance (MR) imaging is a facile and noninvasive imaging technique that offers evident soft tissue contrast and anatomical details [293,294]. The relaxation process in nuclear magnetic resonance can be divided into longitudinal relaxation time (T_1) and transverse relaxation time (T_2), both of which can be employed for MR imaging [295]. Commonly, lanthanide ions such as Gd^{3+} and Yb^{3+} incorporated in the core–shell structured nanoparticles could enhance the contrast in T_1 MR imaging [188,296]. For example, Cai et al. fabricated the UZNPs-PAA-DOX nanoparticles for MR imaging-guided PDT/chemotherapy [84]. As exhibited in the MR images of Fig. 15c, there was no obvious difference between the normal tissue and cancerous tissue before the injection of UZNPs-PAA-DOX nanoparticles, while the cancerous tissue presented brighter image than that of the normal tissue after the injection of UZNPs-PAA-DOX nanoparticles. With the increase of Yb^{3+} ions concentration, the MR signal intensity of UZNPs-PAA-DOX increased gradually. The longitudinal relaxivity of UZNPs-PAA-DOX was estimated to be 10.36 mM^{-1} s^{-1}, indicating its great potential in T_1 MR imaging. Moreover, owing to the unique MR contrast enhancement effect, Fe_3O_4-based core–shell

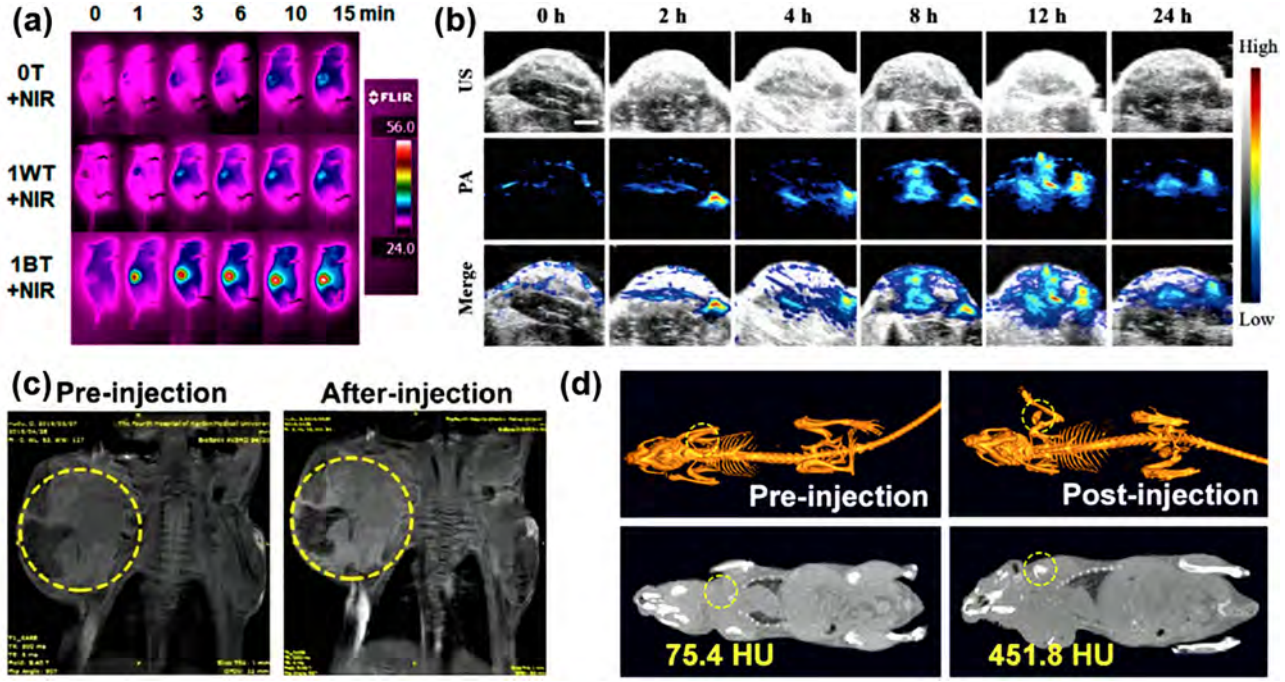

Fig. 15. (a) Infrared thermal images of B16F10 tumor-bearing mice treated with BT-CTS thermogels under the NIR irradiation. Reproduced with permission. [166] Copyright 2019, American Chemical Society. (b) Photoacoustic images of Au@Rh-ICG-CM nanoparticles at the tumor site. Reproduced with permission. [78] Copyright 2020, Wiley-VCH. (c) MR images of mice before and after administration UZNPs-PAA-DOX nanoparticles. Reproduced with permission. [84] Copyright 2020, American Chemical Society. (d) CT images of tumor-bearing mice by pre- and postinjection of PEG/LDNPs@CMSNs nanoparticles. Reproduced with permission. [207] Copyright 2020, American Chemical Society.

structured nanoparticles exhibited excellent performance in T_2 MR imaging [58,105,279].

Recently, Mn- and Fe-containing nanomaterials have drawn much attention as tumor microenvironment-enhanced MR contrast agents [207,297]. In general, the content of GSH, H_2O_2 and H^+ in tumor microenvironment of solid tumor is high. The Mn- and Fe-containing nanomaterials can react with the GSH, H_2O_2 and H^+ in tumor microenvironment to release Mn^{2+} and Fe^{3+} ions for enhancing T_1 and T_2 MR signals, respectively. For example, Xu et al. decorated a mesoporous MnO_2 shell on a UCNPs core for tumor microenvironment-enhanced PDT/chemotherapy and multimodal imaging [298]. In tumor microenvironment, the mesoporous MnO_2 shell decomposed rapidly to release Mn^{2+} ions, which coupled with trimodal imaging of UCNPs to show a self-enhanced imaging. The longitudinal relaxivity of this nanoparticle in PBS was increased from 1.63 (pH 7.4, GSH 0×10^{-3} M, H_2O_2 0×10^{-6} M) to 9.37 mM^{-1} s^{-1} (pH 6.5, GSH 10×10^{-3} M, H_2O_2 50×10^{-6} M). In the study of Ma et al., the Mn^{2+} ions released from SiO_2-MB@MnO_2 nanoparticles due to the decomposition of MnO_2 in acidic tumor microenvironment, which significantly improved the performance of T_1 MR imaging [60].

5.5. Computed tomography imaging

Computed tomography (CT) imaging is an X-ray imaging technique that holds the advantages of fast acquisition time, high resolution and easy three-dimensional modeling [273]. UCNPs-based core–shell structured nanoparticles have attracted much interest as CT contrast agents in PDT-based cancer treatment [59,91,149]. In the study of Wang et al., the UCNPs@mSiO_2-CuS-ZnPc nanoparticles were fabricated for CT imaging-guided PDT [208]. The tumor site without injection of UCNPs@mSiO_2-CuS-ZnPc possessed a CT value of 28.1 Hounsfield Units (HU), which was much lower than the sample-injected tumor site (313.5 HU). Xu et al. investigated the *in vitro* and *in vivo* CT contrast imaging properties of the PEG/LDNPs@CMSNs nanoparticles [207]. As the concentration of PEG/LDNPs@CMSNs nanoparticles increased, the CT signal intensity increased rapidly. As shown in Fig. 15d, the CT value of the tumor site with injection of PEG/LDNPs@CMSNs was 451.8 HU, which was significantly higher than that of the control group (75.4 HU), indicating that the PEG/LDNPs@CMSNs was a promising CT imaging contrast agent.

6. Conclusions and perspectives

In summary, core–shell structured nanoparticles are promising multifunctional nanoplatforms for PDT-based cancer treatment and related imaging. These nanoparticles are divided into three categories: inorganic, organic and hybrid on the basis of material compositions of the core and shell. During PDT of cancer, the core–shell structured nanoparticles serve as photosensitizer delivery vehicles, energy transducers, photosensitizers and hypoxic tumor microenvironment modulators to improve the therapeutic efficacy. The combination of PDT with chemotherapy, PTT, immunotherapy and other therapies resolves some challenging issues for monotherapy, involving the metastasis of tumors and the development of resistance. Moreover, these nanoparticles possess excellent imaging performance in PDT-based cancer treatment.

Despite considerable progress has been made, the core–shell structured nanoparticles are still far from the clinical application of PDT-based cancer treatment and related imaging. From the perspective of materials science, the synthetic steps of most core–shell structured nanoparticles are complex, which easily causes material differences between different batches, and will bring difficulties to the expansion of production and commercialization. Consequently, it is necessary to develop facile synthetic strategies for safely and quickly preparing core–shell structured nanoparticles. Besides, the component of core–shell structured nanoparticles should be optimized for further improving the targeting ability, therapeutic efficacy and stability.

From the perspective of biology, the knowledge of cancers still exists deficiencies because of the limitations of modern technology and the complexity of biosystem. The metastasis of tumors and the development of resistance have always been troubles to be solved urgently for PDT and other therapies. Although many core–shell structured nanoparticles are effective in PDT-based cancer treatment, their systemic cytotoxicity and long-term human toxicity need more comprehensive and in-depth investigation. Meanwhile, the dosage of core–shell structured nanoparticles and light source parameters should be controlled to achieve precise treatment and alleviate side effects. In addition, bacterial infections are one of the inducing factors of cancer and has become increasingly serious with the rise of antibiotic resistance. PDT is a promising strategy to control the bacterial infections, and it is of great significance to develop novel and efficient core–shell structured nanoparticles for antibacterial PDT.

Declaration of Competing Interest

The authors declare that they have no known competing financial interests or personal relationships that could have appeared to influence the work reported in this paper.

Acknowledgements

This study was financially supported by the Program for the National Natural Science Foundation of China (82003363, 82073449, U20A20323, 51521006), the National Program for Support of Top-Notch Young Professionals of China (2014), the Program for Changjiang Scholars and Innovative Research Team in University (IRT-13R17), the Hunan Provincial Science and Technology Plan Project (2018SK20410), the Science and Technology Innovation Program of Hunan Province (2020RC4014), the Changsha Municipal Natural Science Foundation (kq2007059), the Hunan Provincial Natural Science Foundation of China (S2021JJQNJJ2330) and the Shanghai Tongji Gao Tingyao Environmental Science and Technology Development Foundation.

References

[1] H. Sung, J. Ferlay, R.L. Siegel, M. Laversanne, I. Soerjomataram, A. Jemal, F. Bray, CA Cancer J. Clin. 71 (2021) 209–249.
[2] D. Peer, J.M. Karp, S. Hong, O.C. Farokhzad, R. Margalit, R. Langer, Nat. Nanotechnol. 2 (2007) 751–760.
[3] P. Sharma, J.P. Allison, Cell 161 (2015) 205–214.
[4] O. Demaria, S. Cornen, M. Daëron, Y. Morel, R. Medzhitov, E. Vivier, Nature 574 (2019) 45–56.
[5] A.L. Vahrmeijer, M. Hutteman, J.R. Van Der Vorst, C.J. Van De Velde, J.V. Frangioni, Nat. Rev. Clin. Oncol. 10 (2013) 507–518.
[6] A.J. Breugom, M. Swets, J.-F. Bosset, L. Collette, A. Sainato, L. Cionini, R. Glynne-Jones, N. Counsell, E. Bastiaannet, C.B. van den Broek, Lancet Oncol. 16 (2015) 200–207.
[7] L. Kelland, Nat. Rev. Cancer 7 (2007) 573–584.
[8] L. Gandhi, D. Rodríguez-Abreu, S. Gadgeel, E. Esteban, E. Felip, F. De Angelis, M. Domine, P. Clingan, M.J. Hochmair, S.F. Powell, N. Engl, J. Med. 378 (2018) 2078–2092.
[9] A.C. Begg, F.A. Stewart, C. Vens, Nat. Rev. Cancer 11 (2011) 239–253.
[10] C.C. Parker, N.D. James, C.D. Brawley, N.W. Clarke, A.P. Hoyle, A. Ali, A.W. Ritchie, G. Attard, S. Chowdhury, W. Cross, Lancet 392 (2018) 2353–2366.
[11] D.E. Dolmans, D. Fukumura, R.K. Jain, Nat. Rev. Cancer 3 (2003) 380–387.
[12] A.P. Castano, P. Mroz, M.R. Hamblin, Nat. Rev. Cancer 6 (2006) 535–545.
[13] H. Chen, J. Tian, W. He, Z. Guo, J. Am. Chem. Soc. 137 (2015) 1539–1547.
[14] S. Li, H. Cheng, B. Xie, W. Qiu, J. Zeng, C. Li, S. Wan, L. Zhang, W. Liu, X. Zhang, ACS Nano 11 (2017) 7006–7018.
[15] D. Cui, J. Huang, X. Zhen, J. Li, Y. Jiang, K. Pu, Angew. Chem. Int. Ed. 131 (2019) 5981–5985.

[16] P. Agostinis, K. Berg, K.A. Cengel, T.H. Foster, A.W. Girotti, S.O. Gollnick, S.M. Hahn, M.R. Hamblin, A. Juzeniene, D. Kessel, CA Cancer J. Clin. 61 (2011) 250–281.
[17] Z. Zhou, J. Song, L. Nie, X. Chen, Chem. Soc. Rev. 45 (2016) 6597–6626.
[18] T.J. Dougherty, G. Grindey, R. Fiel, K.R. Weishaupt, D. Boyle, J. Natl Cancer Inst. 55 (1975) 115–121.
[19] S.B. Brown, E.A. Brown, I. Walker, Lancet Oncol. 5 (2004) 497–508.
[20] D. Van Straten, V. Mashayekhi, H.S. De Bruijn, S. Oliveira, D.J. Robinson, Cancers 9 (2017) 19.
[21] X. Li, J.F. Lovell, J. Yoon, X. Chen, Nat. Rev. Clin. Oncol. 17 (2020) 657–674.
[22] X. Li, S. Lee, J. Yoon, Chem. Soc. Rev. 47 (2018) 1174–1188.
[23] T.C. Pham, V.-N. Nguyen, Y. Choi, S. Lee, J. Yoon, Chem. Rev. 121 (2021) 13454–13619.
[24] J. Hu, Y.a. Tang, A.H. Elmenoufy, H. Xu, Z. Cheng, X. Yang, Small 11 (2015) 5860–5887.
[25] X. Li, N. Kwon, T. Guo, Z. Liu, J. Yoon, Angew. Chem. Int. Ed. 57 (2018) 11522–11531.
[26] L. Huang, S. Zhao, J. Wu, L. Yu, N. Singh, K. Yang, M. Lan, P. Wang, J.S. Kim, Coord. Chem. Rev. 438 (2021) 213888.
[27] D.K. Chatterjee, L.S. Fong, Y. Zhang, Adv. Drug Deliv. Rev. 60 (2008) 1627–1637.
[28] S.S. Lucky, K.C. Soo, Y. Zhang, Chem. Rev. 115 (2015) 1990–2042.
[29] M. Lismont, L. Dreesen, S. Wuttke, Adv. Funct. Mater. 27 (2017) 1606314.
[30] H. Wang, Y. Wu, T. Xiao, X. Yuan, G. Zeng, W. Tu, S. Wu, H.Y. Lee, Y.Z. Tan, J.W. Chew, Appl. Catal. B: Environ. 233 (2018) 213–225.
[31] D. He, C. Zhang, G. Zeng, Y. Yang, D. Huang, L. Wang, H. Wang, Appl. Catal. B: Environ. 258 (2019) 117957.
[32] Y. Yang, C. Zhou, W. Wang, W. Xiong, G. Zeng, D. Huang, C. Zhang, B. Song, W. Xue, X. Li, Chem. Eng. J. 405 (2021) 126547.
[33] L. Tang, H. Feng, J. Tang, G. Zeng, Y. Deng, J. Wang, Y. Liu, Y. Zhou, Water Res. 117 (2017) 175–186.
[34] H. Feng, L. Tang, J. Tang, G. Zeng, H. Dong, Y. Deng, L. Wang, Y. Liu, X. Ren, Y. Zhou, Environ. Sci: Nano 5 (2018) 1595–1607.
[35] D. Li, C. Li, A. Wang, Q. He, J. Li, J. Mater. Chem. 20 (2010) 7782–7787.
[36] J. Zhao, J. Fei, C. Du, W. Cui, H. Ma, J. Li, Chem. Commun. 49 (2013) 10733–10735.
[37] F. Lu, L. Yang, Y. Ding, J.J. Zhu, Adv. Funct. Mater. 26 (2016) 4778–4785.
[38] N.M. Idris, M.K. Gnanasammandhan, J. Zhang, P.C. Ho, R. Mahendran, Y. Zhang, Nat. Med. 18 (2012) 1580–1585.
[39] Z. Yu, W. Pan, N. Li, B. Tang, Chem. Sci. 7 (2016) 4237–4244.
[40] M. Huo, P. Liu, L. Zhang, C. Wei, L. Wang, Y. Chen, J. Shi, Adv. Funct. Mater. 31 (2021) 2010196.
[41] Y. Li, Z. Di, J. Gao, P. Cheng, C. Di, G. Zhang, B. Liu, X. Shi, L. Sun, L. Li, J. Am. Chem. Soc. 139 (2017) 13804–13810.
[42] Y. Shao, B. Liu, Z. Di, G. Zhang, L. Sun, L. Li, C. Yan, J. Am. Chem. Soc. 142 (2020) 3939–3946.
[43] Z. Wang, B. Liu, Q. Sun, L. Feng, F. He, P. Yang, S. Gai, Z. Quan, J. Lin, ACS Nano 15 (2021) 12342–12357.
[44] R. Lv, P. Yang, F. He, S. Gai, G. Yang, Y. Dai, Z. Hou, J. Lin, Biomaterials 63 (2015) 115–127.
[45] Y. Liu, J. Zhang, C. Zuo, Z. Zhang, D. Ni, C. Zhang, J. Wang, H. Zhang, Z. Yao, W. Bu, Nano Res. 9 (2016) 3257–3266.
[46] A. Skripka, V. Karabanovas, G. Jarockyte, R. Marin, V. Tam, M. Cerruti, R. Rotomskis, F. Vetrone, Adv. Funct. Mater. 29 (2019) 1807105.
[47] F. Chen, B. Madajewski, K. Ma, D.K. Zanoni, H. Stambuk, M.Z. Turker, S. Monette, L. Zhang, B. Yoo, P. Chen, Sci. Adv., 5 (2019) eaax5208.
[48] M. Walczak, R.A. Brady, L. Mancini, C. Contini, R. Rubio-Sánchez, W.T. Kaufhold, P. Cicuta, L. Di Michele, Nat. Commun. 12 (2021) 1–11.
[49] C. Niether, S. Faure, A. Bordet, J. Deseure, M. Chatenet, J. Carrey, B. Chaudret, A. Rouet, Nature Energy 3 (2018) 476–483.
[50] Z. Li, R. Wang, J. Xue, X. Xing, C. Yu, T. Huang, J. Chu, K. Wang, C. Dong, Z. Wei, J. Am. Chem. Soc. 141 (2019) 17610–17616.
[51] S. Das, J. Pérez-Ramírez, J. Gong, N. Dewangan, K. Hidajat, B.C. Gates, S. Kawi, Chem. Soc. Rev. 49 (2020) 2937–3004.
[52] X. Zhang, S. Han, B. Zhu, G. Zhang, X. Li, Y. Gao, Z. Wu, B. Yang, Y. Liu, W. Baaziz, Nature Catalysis 3 (2020) 411–417.
[53] R. Ghosh Chaudhuri, S. Paria, Chem. Rev. 112 (2012) 2373–2433.
[54] M.B. Gawande, A. Goswami, T. Asefa, H. Guo, A.V. Biradar, D.-L. Peng, R. Zboril, R.S. Varma, Chem. Soc. Rev. 44 (2015) 7540–7590.
[55] H. Su, Q. Tian, C.-A.-H. Price, L. Xu, K. Qian, J. Liu, Nano Today 31 (2020) 100834.
[56] M. Tang, X. Zhu, Y. Zhang, Z. Zhang, Z. Zhang, Q. Mei, J. Zhang, M. Wu, J. Liu, Y. Zhang, ACS Nano 13 (2019) 10405–10418.
[57] C. Qin, J. Fei, A. Wang, Y. Yang, J. Li, Nanoscale 7 (2015) 20197–20210.
[58] F. Wang, X. Chen, Z. Zhao, S. Tang, X. Huang, C. Lin, C. Cai, N. Zheng, J. Mater. Chem. 21 (2011) 11244–11252.
[59] Z. Hou, Y. Zhang, K. Deng, Y. Chen, X. Li, X. Deng, Z. Cheng, H. Lian, C. Li, J. Lin, ACS Nano 9 (2015) 2584–2599.
[60] Z. Ma, X. Jia, J. Bai, Y. Ruan, C. Wang, J. Li, M. Zhang, X. Jiang, Adv. Funct. Mater. 27 (2017) 1604258.
[61] X. Huang, G. Deng, Y. Han, G. Yang, R. Zou, Z. Zhang, S. Sun, J. Hu, Adv. Sci. 6 (2019) 1901461.
[62] A. Punjabi, X. Wu, A. Tokatli-Apollon, M. El-Rifai, H. Lee, Y. Zhang, C. Wang, Z. Liu, E.M. Chan, C. Duan, ACS Nano 8 (2014) 10621–10630.
[63] D. Chen, Q. Yu, X. Huang, H. Dai, T. Luo, J. Shao, P. Chen, J. Chen, W. Huang, X. Dong, Small 16 (2020) 2001059.
[64] E. Chang, J. Bu, L. Ding, J.W. Lou, M.S. Valic, M.H. Cheng, V. Rosilio, J. Chen, G. Zheng, J. Nanobiotechnol. 19 (2021) 1–15.
[65] H. Ren, J. Liu, F. Su, S. Ge, A. Yuan, W. Dai, J. Wu, Y. Hu, ACS Appl. Mater. Interfaces 9 (2017) 3463–3473.
[66] P. Liu, Y. Peng, Y. Zhou, X. Shi, Q. Li, J. Ding, Y. Gao, W. Zhou, ACS Appl. Mater. Interfaces 13 (2021) 25674–25684.
[67] G. Dai, C.K.K. Choi, Y. Zhou, Q. Bai, Y. Xiao, C. Yang, C.H.J. Choi, D.K. Ng, Nanoscale 13 (2021) 6499–6512.
[68] X. Tan, J. Wang, X. Pang, L. Liu, Q. Sun, Q. You, F. Tan, N. Li, ACS Appl. Mater. Interfaces 8 (2016) 34991–35003.
[69] J. Feng, W. Ren, J. Gao, F. Li, F. Kong, B. Yao, Y. Dong, ACS Appl. Mater. Interfaces 13 (2021) 17243–17254.
[70] L. Feng, F. He, B. Liu, G. Yang, S. Gai, P. Yang, C. Li, Y. Dai, R. Lv, J. Lin, Chem. Mater. 28 (2016) 7935–7946.
[71] S. Yan, X. Zeng, Y.a. Tang, B. Liu, Y. Wang, X. Liu, Adv. Mater. 31 (2019) 1905825.
[72] H. Zhu, J. Li, X. Qi, P. Chen, K. Pu, Nano Lett. 18 (2018) 586–594.
[73] J. Zeng, M. Zhang, M. Peng, D. Gong, X. Zhang, Adv. Funct. Mater. 28 (2018) 1705451.
[74] S. Ren, B. Wang, X. Zhu, D. Zhu, M. Liu, S. Li, Y. Yang, Z. Wang, H. Zhu, ACS Appl. Mater. Interfaces 12 (2020) 24662–24674.
[75] P. Zhang, W. Steelant, M. Kumar, M. Scholfield, J. Am. Chem. Soc. 129 (2007) 4526–4527.
[76] R. Lv, Y. Wang, J. Liu, M. Feng, F. Yang, X. Jiang, J. Tian, A.C.S. Biomater, Sci. Eng. 5 (2019) 3100–3110.
[77] S.-H. Seo, B.-M. Kim, A. Joe, H.-W. Han, X. Chen, Z. Cheng, E.-S. Jang, Biomaterials 35 (2014) 3309–3318.
[78] J. Wang, J. Sun, W. Hu, Y. Wang, T. Chou, B. Zhang, Q. Zhang, L. Ren, H. Wang, Adv. Mater. 32 (2020) 2001862.
[79] C.W. Lai, Y.H. Wang, C.H. Lai, M.J. Yang, C.Y. Chen, P.T. Chou, C.S. Chan, Y. Chi, Y.C. Chen, J.K. Hsiao, Small 4 (2008) 218–224.
[80] Q. Yu, J. Sun, X. Zhu, L. Qiu, M. Xu, S. Liu, J. Ouyang, J. Liu, J. Mater. Chem. B 5 (2017) 6081–6096.
[81] L. Zeng, H. Zhao, Y. Zhu, S. Chen, Y. Zhang, D. Wei, J. Sun, H. Fan, J. Mater. Chem. B 8 (2020) 4093–4105.
[82] J. Zhu, W. Wang, X. Wang, L. Zhong, X. Song, W. Wang, Y. Zhao, X. Dong, Adv. Healthc. Mater. 10 (2021) 2002038.
[83] S. Ma, J. Xie, L. Wang, Z. Zhou, X. Luo, J. Yan, G. Ran, ACS Appl. Mater. Interfaces 13 (2021) 10728–10740.
[84] Q. Cai, D. Yang, L. Zhong, P. Yang, Chem. Mater. 32 (2020) 7492–7506.
[85] T. Zhao, K. Yu, L. Li, T. Zhang, Z. Guan, N. Gao, P. Yuan, S. Li, S. Yao, Q. Xu, ACS Appl. Mater. Interfaces 6 (2014) 2700–2708.
[86] Y. Wang, H. Gu, Adv. Mater. 27 (2015) 576–585.
[87] M.C. Grüner, M.S. Arai, M. Carreira, N. Inada, A.S. de Camargo, ACS Appl. Bio Mater. 1 (2018) 1028–1036.
[88] J. Xu, P. Yang, M. Sun, H. Bi, B. Liu, D. Yang, S. Gai, F. He, J. Lin, ACS Nano 11 (2017) 4133–4144.
[89] G. Yang, D. Yang, P. Yang, R. Lv, C. Li, C. Zhong, F. He, S. Gai, J. Lin, Chem. Mater. 27 (2015) 7957–7968.
[90] B. Wei, F. Dong, W. Yang, C. Luo, Q. Dong, Z. Zhou, Z. Yang, L. Sheng, J. Adv. Res. 23 (2020) 13–23.
[91] Q. Cai, J. Xu, D. Yang, Y. Dai, G. Yang, C. Zhong, S. Gai, F. He, P. Yang, J. Mater. Chem. B 6 (2018) 8148–8162.
[92] X. Zhu, Y. Liu, G. Yuan, X. Guo, J. Cen, Y. Gong, J. Liu, Y. Gang, Nanoscale 12 (2020) 22317–22329.
[93] L. Feng, S. Gai, F. He, Y. Dai, C. Zhong, P. Yang, J. Lin, Biomaterials 147 (2017) 39–52.
[94] X. Qiao, J. Zhou, J. Xiao, Y. Wang, L. Sun, C. Yan, Nanoscale 4 (2012) 4611–4623.
[95] S.S. Lucky, N. Muhammad Idris, Z. Li, K. Huang, K.C. Soo, Y. Zhang, ACS Nano 9 (2015) 191–205.
[96] P. Liu, Y. Zhou, X. Shi, Y. Yuan, Y. Peng, S. Hua, Q. Luo, J. Ding, Y. Li, W. Zhou, J. Nanobiotechnol. 19 (2021) 1–13.
[97] Q. Li, J. Ren, Q. Chen, W. Liu, Z. Xu, Y. Cao, Y. Kang, P. Xue, Nanoscale 12 (2020) 12508–12521.
[98] Z. Chen, M. Niu, G. Chen, Q. Wu, L. Tan, C. Fu, X. Ren, H. Zhong, K. Xu, X. Meng, ACS Nano 12 (2018) 12721–12732.
[99] J. Shen, G. Chen, T.Y. Ohulchanskyy, S.J. Kesselli, S. Buchholz, Z. Li, P.N. Prasad, G. Han, Small 9 (2013) 3213–3217.
[100] Q. Yu, A. Xie, Y. Xiao, S. Li, F. Huang, Y. Shen, J. Mater. Chem. B 3 (2015) 1439–1445.
[101] H. Jia, Y. Jiang, Y. Zhu, Y. Li, H. Wang, X. Han, Z. Yu, N. Gu, P. Liu, Z. Chen, J. Controlled Release 255 (2017) 231–241.
[102] W.L. Kim, H. Cho, L. Li, H.C. Kang, K.M. Huh, Biomacromolecules 15 (2014) 2224–2234.
[103] H. An, C. Guo, D. Li, R. Liu, X. Xu, J. Guo, J. Ding, J. Li, W. Chen, J. Zhang, ACS Appl. Mater. Interfaces 12 (2020) 17230–17243.
[104] Y. Cheng, H. Cheng, C. Jiang, X. Qiu, K. Wang, W. Huan, A. Yuan, J. Wu, Y. Hu, Nat. Commun. 6 (2015) 1–8.
[105] L. Feng, D. Yang, F. He, S. Gai, C. Li, Y. Dai, P. Yang, Adv. Healthc. Mater. 6 (2017) 1700502.
[106] X. Zhang, F. Ai, T. Sun, F. Wang, G. Zhu, Inorg. Chem. 55 (2016) 3872–3880.
[107] H. Wang, Z. Wang, Y. Li, T. Xu, Q. Zhang, M. Yang, P. Wang, Y. Gu, Small 15 (2019) 1902185.
[108] X. Zhang, J. Ong'achwa Machuki, W. Pan, W. Cai, Z. Xi, F. Shen, L. Zhang, Y. Yang, F. Gao, M. Guan, ACS Nano, 14 (2020) 4045-4060.

[109] C. Zhang, W. Chen, T. Zhang, X. Jiang, Y. Hu, J. Mater. Chem. B 8 (2020) 4726–4737.
[110] C. Liang, X. Zhang, Z. Wang, W. Wang, M. Yang, X. Dong, J. Mater. Chem. B 8 (2020) 4748–4763.
[111] J. Xu, R. Lv, S. Du, S. Gai, F. He, D. Yang, P. Yang, J. Mater. Chem. B 4 (2016) 4138–4146.
[112] W. Liu, Y. Tian, Y. Zhang, K. Liu, S. Zhao, J. Zhang, Y. Su, Y. Zhao, Y. Tang, J. Sun, J. Mater. Chem. B 6 (2018) 3865–3875.
[113] H. Cai, T. Shen, J. Zhang, C. Shan, J. Jia, X. Li, W. Liu, Y. Tang, J. Mater. Chem. B 5 (2017) 2390–2394.
[114] J. Shen, M. Ma, H. Zhang, H. Yu, F. Xue, N. Hao, H. Chen, ACS Appl. Mater. Interfaces 12 (2020) 45838–45849.
[115] S. Ren, X. Zhu, B. Wang, M. Liu, S. Li, Y. Yang, H. An, H. Zhu, J. Mater. Chem. B 9 (2021) 4678–4689.
[116] J. Liu, L. Ye, W. Xiong, T. Liu, H. Yang, J. Lei, Chem. Commun. 57 (2021) 2820–2823.
[117] M. Lan, S. Zhao, W. Liu, C.S. Lee, W. Zhang, P. Wang, Adv. Healthc. Mater. 8 (2019) 1900132.
[118] X. Yang, Q. Xiao, C. Niu, N. Jin, J. Ouyang, X. Xiao, D. He, J. Mater. Chem. B 1 (2013) 2757–2763.
[119] S. Bouramtane, L. Bretin, A. Pinon, D. Leger, B. Liagre, L. Richard, F. Brégier, V. Sol, V. Chaleix, Carbohydr. Polym. 213 (2019) 168–175.
[120] Y. Cui, G. Sun, Y. Li, A. Tang, L. Zhu, D. Kong, Adv. Mater. Interfaces 7 (2020) 2000292.
[121] R. Jenjob, T. Phakkeeree, D. Crespy, Biomater. Sci. 8 (2020) 2756–2770.
[122] J. Tan, C. Sun, K. Xu, C. Wang, J. Guo, Small 11 (2015) 6338–6346.
[123] P. Yang, S. Gai, J. Lin, Chem. Soc. Rev. 41 (2012) 3679–3698.
[124] G. Yang, X. Sun, J. Liu, L. Feng, Z. Liu, Adv. Funct. Mater. 26 (2016) 4722–4732.
[125] H. Qian, H. Guo, P.C.L. Ho, R. Mahendran, Y. Zhang, Small 5 (2009) 2285–2290.
[126] W. Zeng, H. Zhang, Y. Deng, A. Jiang, X. Bao, M. Guo, Z. Li, M. Wu, X. Ji, X. Zeng, Chem. Eng. J. 389 (2020) 124494.
[127] C. Conte, F. Ungaro, G. Maglio, P. Tirino, G. Siracusano, M. Sciortino, N. Leone, G. Palma, A. Barbieri, C. Arra, J. Controlled Release 167 (2013) 40–52.
[128] B. Sun, Y. Chen, H. Yu, C. Wang, X. Zhang, H. Zhao, Q. Chen, Z. He, C. Luo, J. Sun, Acta Biomater. 92 (2019) 219–228.
[129] P. Liu, X. Xie, X. Shi, Y. Peng, J. Ding, W. Zhou, ACS Appl. Mater. Interfaces 11 (2019) 48261–48270.
[130] J. Wang, Y. Zhong, X. Wang, W. Yang, F. Bai, B. Zhang, L. Alarid, K. Bian, H. Fan, Nano Lett. 17 (2017) 6916–6921.
[131] J. Yoo, C. Park, G. Yi, D. Lee, H. Koo, Cancers 11 (2019) 640.
[132] P.S. Low, W.A. Henne, D.D. Doorneweerd, Acc. Chem. Res. 41 (2008) 120–129.
[133] F. Danhier, O. Feron, V. Préat, J. Controlled Release 148 (2010) 135–146.
[134] S. Liang, C. Sun, P. Yang, S. Huang, Z. Cheng, X. Yu, J. Lin, Biomaterials 240 (2020) 119850.
[135] R. Luo, Z. Zhang, L. Han, Z. Xue, K. Zhang, F. Liu, F. Feng, J. Xue, W. Liu, W. Qu, Biomater. Sci. 9 (2021) 3718–3736.
[136] Q. Meng, J. Meng, W. Ran, J. Wang, Y. Zhai, P. Zhang, Y. Li, ACS Nano 12 (2018) 2789–2802.
[137] B. Wang, W. Lin, Z. Mao, C. Gao, J. Mater. Chem. B 6 (2018) 3145–3155.
[138] D. Chen, Q. Xu, W. Wang, J. Shao, W. Huang, X. Dong, Small 17 (2021) 2006742.
[139] R. Vankayala, K.C. Hwang, Adv. Mater. 30 (2018) 1706320.
[140] Z. Gu, L. Yan, G. Tian, S. Li, Z. Chai, Y. Zhao, Adv. Mater. 25 (2013) 3758–3779.
[141] Y. Liu, X. Meng, W. Bu, Coord. Chem. Rev. 379 (2019) 82–98.
[142] S. Ding, W. Wu, T. Peng, W. Pang, P. Jiang, Q. Zhan, S. Qi, X. Wei, B. Gu, B. Liu, Nanoscale Adv. 3 (2021) 2325–2333.
[143] Y.I. Park, H.M. Kim, J.H. Kim, K.C. Moon, B. Yoo, K.T. Lee, N. Lee, Y. Choi, W. Park, D. Ling, Adv. Mater. 24 (2012) 5755–5761.
[144] S. Wu, H.J. Butt, Adv. Mater. 28 (2016) 1208–1226.
[145] G. Tan, M. Wang, C. Hsu, N. Chen, Y. Zhang, Adv. Opt. Mater. 4 (2016) 984–997.
[146] M. Yang, H. Wang, Z. Wang, Z. Han, Y. Gu, Biomater. Sci. 7 (2019) 1686–1695.
[147] T. Shen, X. Hu, Y. Liu, Y. Zhang, K. Chen, S. Xie, G. Ke, G. Song, X. Zhang, A.C.S. Appl, Mater. Interfaces 12 (2020) 5403–5412.
[148] S.-L. Lin, C.A. Chang, Nanoscale 12 (2020) 8742–8749.
[149] W. Park, S. Cho, D. Kang, J.H. Han, J.H. Park, B. Lee, J. Lee, D.H. Kim, Adv. Healthc. Mater. 9 (2020) 1901812.
[150] Y. Ren, J.G. Rosch, M.R. Landry, H. Winter, S. Khan, G. Pratx, C. Sun, Biomater. Sci. 9 (2021) 496–505.
[151] A. Kamkaew, F. Chen, Y. Zhan, R.L. Majewski, W. Cai, ACS Nano 10 (2016) 3918–3935.
[152] W. Sun, Z. Zhou, G. Pratx, X. Chen, H. Chen, Theranostics 10 (2020) 1296.
[153] C. Zhang, K. Zhao, W. Bu, D. Ni, Y. Liu, J. Feng, J. Shi, Angew. Chem. Int. Ed. 54 (2015) 1770–1774.
[154] Y.a. Tang, J. Hu, A.H. Elmenoufy, X. Yang, ACS Appl. Mater. Interfaces, 7 (2015) 12261-12269.
[155] C.-C. Hsu, S.-L. Lin, C.A. Chang, ACS Appl. Mater. Interfaces 10 (2018) 7859–7870.
[156] R. Lv, P. Yang, F. He, S. Gai, C. Li, Y. Dai, G. Yang, J. Lin, Acs Nano 9 (2015) 1630–1647.
[157] L. Lin, J. Song, H. Yang, X. Chen, Adv. Mater. 30 (2018) 1704639.
[158] J. Wang, N. Li, J. Mater. Chem. B 5 (2017) 8430–8445.
[159] W. Wang, C. Huang, C. Zhang, M. Zhao, J. Zhang, H. Chen, Z. Zha, T. Zhao, H. Qian, Appl. Catal. B: Environ. 224 (2018) 854–862.
[160] Y. Chang, Y. Cheng, Y. Feng, H. Jian, L. Wang, X. Ma, X. Li, H. Zhang, Nano Lett. 18 (2018) 886–897.
[161] A. Kamkaew, L. Cheng, S. Goel, H.F. Valdovinos, T.E. Barnhart, Z. Liu, W. Cai, ACS Appl. Mater. Interfaces 8 (2016) 26630–26637.
[162] D. Yang, G. Yang, Q. Sun, S. Gai, F. He, Y. Dai, C. Zhong, P. Yang, Adv. Healthc. Mater. 7 (2018) 1800042.
[163] W. Guo, F. Wang, D. Ding, C. Song, C. Guo, S. Liu, Chem. Mater. 29 (2017) 9262–9274.
[164] W. Chen, X. Wang, B. Zhao, R. Zhang, Z. Xie, Y. He, A. Chen, X. Xie, K. Yao, M. Zhong, Nanoscale 11 (2019) 12983–12989.
[165] C. Liu, H. Dong, N. Wu, Y. Cao, X. Zhang, ACS Appl. Mater. Interfaces 10 (2018) 6991–7002.
[166] X. Wang, B. Ma, J. Xue, J. Wu, J. Chang, C. Wu, Nano Lett. 19 (2019) 2138–2147.
[167] H. Taheri, M.A. Unal, M. Sevim, C. Gurcan, O. Ekim, A. Ceylan, Z. Syrgiannis, K. C. Christoforidis, S. Bosi, O. Ozgenç, Small 16 (2020) 1904619.
[168] H. Liu, X. Lv, J. Qian, H. Li, Y. Qian, X. Wang, X. Meng, W. Lin, H. Wang, ACS Nano 14 (2020) 13304–13315.
[169] W. Zhang, S. Li, X. Liu, C. Yang, N. Hu, L. Dou, B. Zhao, Q. Zhang, Y. Suo, J. Wang, Adv. Funct. Mater. 28 (2018) 1706375.
[170] Y. Yang, X. Li, C. Zhou, W. Xiong, G. Zeng, D. Huang, C. Zhang, W. Wang, B. Song, X. Tang, Water Res. 184 (2020) 116200.
[171] Y. Yang, G. Zeng, D. Huang, C. Zhang, D. He, C. Zhou, W. Wang, W. Xiong, B. Song, H. Yi, Small 16 (2020) 2001634.
[172] J. Park, Q. Jiang, D. Feng, L. Mao, H. Zhou, J. Am. Chem. Soc. 138 (2016) 3518–3525.
[173] G. Lan, K. Ni, R. Xu, K. Lu, Z. Lin, C. Chan, W. Lin, Angew. Chem. Int. Ed. 129 (2017) 12270–12274.
[174] G. Lan, K. Ni, Z. Xu, S.S. Veroneau, Y. Song, W. Lin, J. Am. Chem. Soc. 140 (2018) 5670–5673.
[175] J.M. Brown, W.R. Wilson, Nat. Rev. Cancer 4 (2004) 437–447.
[176] W.R. Wilson, M.P. Hay, Nat. Rev. Cancer 11 (2011) 393–410.
[177] L. Larue, B. Myrzakhmetov, A. Ben-Mihoub, A. Moussaron, N. Thomas, P. Arnoux, F. Baros, R. Vanderesse, S. Acherar, C. Frochot, Pharmaceuticals 12 (2019) 163.
[178] F. Wei, T.W. Rees, X. Liao, L. Ji, H. Chao, Coord. Chem. Rev. 432 (2021) 213714.
[179] D.M. Gilkes, G.L. Semenza, D. Wirtz, Nat. Rev. Cancer 14 (2014) 430–439.
[180] Z. Shen, Q. Ma, X. Zhou, G. Zhang, G. Hao, Y. Sun, J. Cao, NPG Asia Materials 13 (2021) 1–19.
[181] L. Han, Y. Wang, X. Huang, F. Liu, C. Ma, F. Feng, J. Zhang, W. Liu, W. Qu, H. Pang, Biomaterials 257 (2020) 120228.
[182] J. Zheng, J. Sun, J. Chen, S. Zhu, S. Chen, Y. Liu, L. Hao, Z. Wang, S. Chang, J. Controlled Release 332 (2021) 448–459.
[183] H. Cheng, X. Wang, X. Liu, X. Wang, H. Wen, Y. Cheng, A. Xie, Y. Shen, R. Tang, M. Zhu, Nanoscale 13 (2021) 10816–10828.
[184] Y. Lan, X. Zhu, M. Tang, Y. Wu, J. Zhang, J. Liu, Y. Zhang, Nanoscale 12 (2020) 7875–7887.
[185] R.A. Day, E.M. Sletten, Curr. Opin. Colloid In. 54 (2021) 101454.
[186] J.B. DeCoste, M.H. Weston, P.E. Fuller, T.M. Tovar, G.W. Peterson, M.D. LeVan, O.K. Farha, Angew. Chem. Int. Ed. 126 (2014) 14316–14319.
[187] P.Z. Moghadam, T. Islamoglu, S. Goswami, J. Exley, M. Fantham, C.F. Kaminski, R.Q. Snurr, O.K. Farha, D. Fairen-Jimenez, Nat. Commun. 9 (2018) 1–8.
[188] Z. Xie, X. Cai, C. Sun, S. Liang, S. Shao, S. Huang, Z. Cheng, M. Pang, B. Xing, A.A. A. Kheraif, Chem. Mater. 31 (2018) 483–490.
[189] Y. Zhang, D. Wang, Y. Meng, W. Lu, S. Shuang, C. Dong, A.C.S. Sustain, Chem. Eng. 9 (2021) 2770–2783.
[190] X. Zhang, Z. Xi, J.O.a. Machuki, J. Luo, D. Yang, J. Li, W. Cai, Y. Yang, L. Zhang, J. Tian, ACS Nano, 13 (2019) 5306-5325.
[191] Y. Song, Q. Shi, C. Zhu, Y. Luo, Q. Lu, H. Li, R. Ye, D. Du, Y. Lin, Nanoscale 9 (2017) 15813–15824.
[192] Y. Li, X. Jian, S. Zhou, Y. Lu, C. Zhao, Z. Gao, Y. Song, ACS Appl. Mater. Interfaces 11 (2019) 17215–17225.
[193] H. Cao, Y. Yang, M. Liang, Y. Ma, N. Sun, X. Gao, J. Li, Chem. Commun. 57 (2021) 255–258.
[194] X. Wang, J. Zeng, M. Zhang, X. Zeng, X. Zhang, Adv. Funct. Mater. 28 (2018) 1801783.
[195] M. Huo, L. Wang, Y. Chen, J. Shi, Nat. Commun. 8 (2017) 1–12.
[196] L. He, Q. Ni, J. Mu, W. Fan, L. Liu, Z. Wang, L. Li, W. Tang, Y. Liu, Y. Cheng, J. Am. Chem. Soc. 142 (2020) 6822–6832.
[197] M. Rizwan, T. Rasheed, A. Raza, M. Bilal, R. Yahya, M. Yar, H.M. Iqbal, J. Drug Deliv. Sci. Tec. 51 (2019) 70–82.
[198] J. Hu, Q. Lei, X. Zhang, Prog. Mater Sci. 114 (2020) 100685.
[199] V. Salgueiriño-Maceira, M.A. Correa-Duarte, Adv. Mater. 19 (2007) 4131–4144.
[200] L. Labrador-Páez, E.C. Ximendes, P. Rodríguez-Sevilla, D.H. Ortgies, U. Rocha, C. Jacinto, E.M. Rodríguez, P. Haro-González, D. Jaque, Nanoscale 10 (2018) 12935–12956.
[201] C. He, D. Liu, W. Lin, ACS Nano 9 (2015) 991–1003.
[202] Z. Zhou, J. Zhao, Z. Di, B. Liu, Z. Li, X. Wu, L. Li, Nanoscale 13 (2021) 131–137.
[203] Y. Gao, L. Zhang, Y. Liu, S. Sun, Z. Yin, L. Zhang, A. Li, G. Lu, A. Wu, L. Zeng, Nanoscale 12 (2020) 1801–1810.
[204] C. Yang, Y. Zhu, D. Li, Y. Liu, C. Guan, X. Man, S. Zhang, L. Zhang, D. Yang, Y. Xu, Small 17 (2021) 2101837.
[205] X. Duan, C. Chan, N. Guo, W. Han, R.R. Weichselbaum, W. Lin, J. Am. Chem. Soc. 138 (2016) 16686–16695.
[206] N. Peng, H. Yu, W. Yu, M. Yang, H. Chen, T. Zou, K. Deng, S. Huang, Y. Liu, Acta Biomater. 105 (2020) 223–238.

[207] J. Xu, R. Shi, G. Chen, S. Dong, P. Yang, Z. Zhang, N. Niu, S. Gai, F. He, Y. Fu, ACS Nano 14 (2020) 9613–9625.
[208] Y. Wang, G. Yang, Y. Wang, Y. Zhao, H. Jiang, Y. Han, P. Yang, Nanoscale 9 (2017) 4759–4769.
[209] B.A. Chabner, T.G. Roberts, Nat. Rev. Cancer 5 (2005) 65–72.
[210] V.T. DeVita, E. Chu, Cancer Res. 68 (2008) 8643–8653.
[211] C. Holohan, S. Van Schaeybroeck, D.B. Longley, P.G. Johnston, Nat. Rev. Cancer 13 (2013) 714–726.
[212] J. Zhou, G. Yu, F. Huang, Chem. Soc. Rev. 46 (2017) 7021–7053.
[213] G. Pasparakis, T. Manouras, M. Vamvakaki, P. Argitis, Nat. Commun. 5 (2014) 1–9.
[214] Q. Pei, X. Hu, X. Zheng, S. Liu, Y. Li, X. Jing, Z. Xie, ACS Nano 12 (2018) 1630–1641.
[215] L. Liu, X. Zhou, R. Zheng, J. Huang, R. Kong, Y. Li, C. Wang, A. Chen, S. Li, H. Cheng, Chem. Commun. 57 (2021) 7296–7299.
[216] G. Saravanakumar, J. Lee, J. Kim, W.J. Kim, Chem. Commun. 51 (2015) 9995–9998.
[217] Q. Chen, X. Wang, C. Wang, L. Feng, Y. Li, Z. Liu, ACS Nano 9 (2015) 5223–5233.
[218] D. Yang, J. Xu, G. Yang, Y. Zhou, H. Ji, H. Bi, S. Gai, F. He, P. Yang, Chem. Eng. J. 344 (2018) 363–374.
[219] H. Peng, Y. Qin, X. He, W. Li, Y. Zhang, A.C.S. Appl, Mater. Interfaces 12 (2020) 13360–13370.
[220] M.C. Lukowiak, B.N. Thota, R. Haag, Biotechnol. Adv. 33 (2015) 1327–1341.
[221] R. Kumar, K. Mondal, P.K. Panda, A. Kaushik, R. Abolhassani, R. Ahuja, H.-G. Rubahn, Y.K. Mishra, J. Mater. Chem. B 8 (2020) 8992–9027.
[222] J. Lee, R. Jenjob, E. Davaa, S.-G. Yang, J. Controlled Release 305 (2019) 120–129.
[223] X. Huang, I.H. El-Sayed, W. Qian, M.A. El-Sayed, J. Am. Chem. Soc. 128 (2006) 2115–2120.
[224] P.K. Jain, X. Huang, I.H. El-Sayed, M.A. El-Sayed, Acc. Chem. Res. 41 (2008) 1578–1586.
[225] J. Shao, H. Xie, H. Huang, Z. Li, Z. Sun, Y. Xu, Q. Xiao, X.-F. Yu, Y. Zhao, H. Zhang, Nat. Commun. 7 (2016) 1–13.
[226] R. Jiang, J. Dai, X. Dong, Q. Wang, Z. Meng, J. Guo, Y. Yu, S. Wang, F. Xia, Z. Zhao, Adv. Mater. 33 (2021) 2101158.
[227] X. Deng, Z. Shao, Y. Zhao, Adv. Sci. 8 (2021) 2002504.
[228] Y. Chang, Y. Cheng, R. Zheng, X. Wu, P. Song, Y. Wang, J. Yan, H. Zhang, Nano Today 38 (2021) 101110.
[229] R. Liang, L. Liu, H. He, Z. Chen, Z. Han, Z. Luo, Z. Wu, M. Zheng, Y. Ma, L. Cai, Biomaterials 177 (2018) 149–160.
[230] H. He, L. Liu, R. Liang, H. Zhou, H. Pan, S. Zhang, L. Cai, Acta Biomater. 104 (2020) 188–197.
[231] Y. Pu, Y. Zhu, Z. Qiao, N. Xin, S. Chen, J. Sun, R. Jin, Y. Nie, H. Fan, J. Mater. Chem. B 9 (2021) 1846–1857.
[232] F. He, L. Feng, P. Yang, B. Liu, S. Gai, G. Yang, Y. Dai, J. Lin, Biomaterials 105 (2016) 77–88.
[233] Y. Qi, J. Ye, S. Ren, G. Wang, J. Lv, S. Zhang, Y. Che, Y. Li, B. Chen, G. Ning, Adv. Healthc. Mater. 9 (2020) 2001205.
[234] M. Xu, G. Yang, H. Bi, J. Xu, L. Feng, D. Yang, Q. Sun, S. Gai, F. He, Y. Dai, Chem. Eng. J. 360 (2019) 866–878.
[235] M. Zhang, X. Qin, W. Xu, Y. Wang, Y. Song, S. Garg, Y. Luan, J. Colloid Interface Sci. 594 (2021) 493–501.
[236] B. Jang, J.-Y. Park, C.-H. Tung, I.-H. Kim, Y. Choi, ACS Nano 5 (2011) 1086–1094.
[237] N. Song, Z. Zhang, P. Liu, D. Dai, C. Chen, Y. Li, L. Wang, T. Han, Y. Yang, D. Wang, Adv. Funct. Mater. 31 (2021) 2009924.
[238] Y.K. Kim, H.K. Na, S. Kim, H. Jang, S.J. Chang, D.H. Min, Small 11 (2015) 2527–2535.
[239] Y. Chen, W. Ai, X. Guo, Y. Li, Y. Ma, L. Chen, H. Zhang, T. Wang, X. Zhang, Z. Wang, Small 15 (2019) 1902352.
[240] Y. Xing, T. Ding, Z. Wang, L. Wang, H. Guan, J. Tang, D. Mo, J. Zhang, ACS Appl. Mater. Interfaces 11 (2019) 13945–13953.
[241] Y. Cen, W. Deng, Y. Yang, R. Yu, X. Chu, Anal. Chem. 89 (2017) 10321–10328.
[242] Z. Yang, X. Liu, X. Wang, P. Wang, S. Ruan, A. Xie, Y. Shen, M. Zhu, Chem. Eng. J. 387 (2020) 124113.
[243] W. Cheng, J. Nie, L. Xu, C. Liang, Y. Peng, G. Liu, T. Wang, L. Mei, L. Huang, X. Zeng, ACS Appl. Mater. Interfaces 9 (2017) 18462–18473.
[244] B. Chen, Y. Zhang, R. Ran, B. Wang, F. Qin, T. Zhang, G. Wan, H. Chen, Y. Wang, Polym. Chem. 10 (2019) 4746–4757.
[245] W. Song, J. Kuang, C.-X. Li, M. Zhang, D. Zheng, X. Zeng, C. Liu, X. Zhang, ACS Nano 12 (2018) 1978–1989.
[246] X. Xu, G. Deng, Z. Sun, Y. Luo, J. Liu, X. Yu, Y. Zhao, P. Gong, G. Liu, P. Zhang, Adv. Mater. 33 (2021) 2102322.
[247] J. Zou, L. Li, Z. Yang, X. Chen, Nanophotonics 10 (2021) 3229–3245.
[248] W. Sang, Z. Zhang, Y. Dai, X. Chen, Chem. Soc. Rev. 48 (2019) 3771–3810.
[249] I. Mellman, G. Coukos, G. Dranoff, Nature 480 (2011) 480–489.
[250] M.M. Gubin, X. Zhang, H. Schuster, E. Caron, J.P. Ward, T. Noguchi, Y. Ivanova, J. Hundal, C.D. Arthur, W.-J. Krebber, Nature 515 (2014) 577–581.
[251] A. Ribas, J.D. Wolchok, Science 359 (2018) 1350–1355.
[252] R.M. Webster, Nat. Rev. Drug Discov. 13 (2014) 883.
[253] L. Chen, X. Han, J. Clin. Invest. 125 (2015) 3384–3391.
[254] J. Guo, Q. An, M. Guo, Y. Xiao, B. Li, F. Gao, Y. Wang, J. Li, Y. Wang, Y. Liu, Nano Today 36 (2021) 101024.
[255] C. He, X. Duan, N. Guo, C. Chan, C. Poon, R.R. Weichselbaum, W. Lin, Nat. Commun. 7 (2016) 1–12.
[256] X. Yu, X. Liu, W. Wu, K. Yang, R. Mao, F. Ahmad, X. Chen, W. Li, Angew. Chem. Int. Ed. 131 (2019) 2039–2044.
[257] Q. Wang, N. Liu, Z. Hou, J. Shi, X. Su, X. Sun, Adv. Healthc. Mater. 10 (2021) 2000802.
[258] S.-J. Tseng, Z.-X. Liao, S.-H. Kao, Y.-F. Zeng, K.-Y. Huang, H.-J. Li, C.-L. Yang, Y.-F. Deng, C.-F. Huang, S.-C. Yang, Nat. Commun. 6 (2015) 1–10.
[259] N. Zheng, X. Luo, Z. Zhang, A. Wang, W. Song, ACS Appl. Mater. Interfaces 13 (2021) 27513–27521.
[260] C. Liu, D. Wang, S. Zhang, Y. Cheng, F. Yang, Y. Xing, T. Xu, H. Dong, X. Zhang, ACS Nano 13 (2019) 4267–4277.
[261] S. Wang, G. Yu, W. Yang, Z. Wang, O. Jacobson, R. Tian, H. Deng, L. Lin, X. Chen, Adv. Sci. 8 (2021) 2002927.
[262] D. Schaue, W.H. McBride, Nat. Rev. Clin. Oncol. 12 (2015) 527–540.
[263] J.d.S. Oliveira, E. Guidelli, Mater. Sci. Eng. C 126 (2021) 112122.
[264] N. Somia, I.M. Verma, Nat. Rev. Genet. 1 (2000) 91–99.
[265] M.T. McManus, P.A. Sharp, Nat. Rev. Genet. 3 (2002) 737–747.
[266] M. Izquierdo, Cancer Gene Ther. 12 (2005) 217–227.
[267] L. Feng, R. Xie, C. Wang, S. Gai, F. He, D. Yang, P. Yang, J. Lin, ACS Nano 12 (2018) 11000–11012.
[268] Z. Tang, Y. Liu, M. He, W. Bu, Angew. Chem. Int. Ed. 58 (2019) 946–956.
[269] C. Yao, W. Wang, P. Wang, M. Zhao, X. Li, F. Zhang, Adv. Mater. 30 (2018) 1704833.
[270] Z. Zhao, W. Wang, C. Li, Y. Zhang, T. Yu, R. Wu, J. Zhao, Z. Liu, J. Liu, H. Yu, Adv. Funct. Mater. 29 (2019) 1905013.
[271] J.P. Celli, B.Q. Spring, I. Rizvi, C.L. Evans, K.S. Samkoe, S. Verma, B.W. Pogue, T. Hasan, Chem. Rev. 110 (2010) 2795–2838.
[272] M. Ethirajan, Y. Chen, P. Joshi, R.K. Pandey, Chem. Soc. Rev. 40 (2011) 340–362.
[273] B.R. Smith, S.S. Gambhir, Chem. Rev. 117 (2017) 901–986.
[274] Z. Wang, Q. Sun, B. Liu, Y. Kuang, A. Gulzar, F. He, S. Gai, P. Yang, J. Lin, Coord. Chem. Rev. 439 (2021) 213945.
[275] J. Li, K. Pu, Chem. Soc. Rev. 48 (2019) 38–71.
[276] Y. Wu, M.R. Ali, K. Chen, N. Fang, M.A. El-Sayed, Nano Today 24 (2019) 120–140.
[277] J.F. Lovell, T.W. Liu, J. Chen, G. Zheng, Chem. Rev. 110 (2010) 2839–2857.
[278] I.-H. Oh, H.S. Min, L. Li, T.H. Tran, Y.-K. Lee, I.C. Kwon, K. Choi, K. Kim, K.M. Huh, Biomaterials 34 (2013) 6454–6463.
[279] L. Li, M. Nurunnabi, M. Nafiujjaman, Y.Y. Jeong, Y.-K. Lee, K.M. Huh, J. Mater. Chem. B 2 (2014) 2929–2937.
[280] K.D. Wegner, N. Hildebrandt, Chem. Soc. Rev. 44 (2015) 4792–4834.
[281] J. Shen, L. Zhao, G. Han, Adv. Drug Deliv. Rev. 65 (2013) 744–755.
[282] H. Wang, R. Han, L. Yang, J. Shi, Z. Liu, Y. Hu, Y. Wang, S. Liu, Y. Gan, ACS Appl. Mater. Interfaces 8 (2016) 4416–4423.
[283] S. Zhu, R. Tian, A.L. Antaris, X. Chen, H. Dai, Adv. Mater. 31 (2019) 1900321.
[284] Y. Fan, P. Wang, Y. Lu, R. Wang, L. Zhou, X. Zheng, X. Li, J.A. Piper, F. Zhang, Nat. Nanotechnol. 13 (2018) 941–946.
[285] K.-Y. Pham, L.-C. Wang, C.-C. Hsieh, Y.-P. Hsu, L.-C. Chang, W.-P. Su, Y.-H. Chien, C.-S. Yeh, J. Mater. Chem. B 9 (2021) 694–709.
[286] D. Wang, B. Xue, T.Y. Ohulchanskyy, Y. Liu, A. Yakovliev, R. Ziniuk, M. Xu, J. Song, J. Qu, Z. Yuan, Biomaterials 251 (2020) 120088.
[287] C. Liang, S. Diao, C. Wang, H. Gong, T. Liu, G. Hong, X. Shi, H. Dai, Z. Liu, Adv. Mater. 26 (2014) 5646–5652.
[288] X. Mu, Y. Tang, F. Wu, H. Ma, S. Huang, M. Liang, J. Yang, Y. Lu, X. Zhou, Z. Li, ACS Appl. Mater. Interfaces 13 (2021) 36958–36966.
[289] C. Ou, Y. Zhang, D. Pan, K. Ding, S. Zhang, W. Xu, W. Wang, W. Si, Z. Yang, X. Dong, Mater. Chem. Front. 3 (2019) 1786–1792.
[290] J. Weber, P.C. Beard, S.E. Bohndiek, Nat. Methods 13 (2016) 639–650.
[291] Q. Fu, R. Zhu, J. Song, H. Yang, X. Chen, Adv. Mater. 31 (2019) 1805875.
[292] Y. Liu, P. Bhattarai, Z. Dai, X. Chen, Chem. Soc. Rev. 48 (2019) 2053–2108.
[293] Y.W. Jun, J.H. Lee, J. Cheon, Angew. Chem. Int. Ed. 47 (2008) 5122–5135.
[294] D. Ni, W. Bu, E.B. Ehlerding, W. Cai, J. Shi, Chem. Soc. Rev. 46 (2017) 7438–7468.
[295] Q. Chen, J. Wen, H. Li, Y. Xu, F. Liu, S. Sun, Biomaterials 106 (2016) 144–166.
[296] J. Xu, D. Yang, R. Lv, B. Liu, S. Gai, F. He, C. Li, P. Yang, J. Mater. Chem. B 4 (2016) 5883–5894.
[297] T. Jia, Z. Wang, Q. Sun, S. Dong, J. Xu, F. Zhang, L. Feng, F. He, D. Yang, P. Yang, Small 16 (2020) 2001343.
[298] J. Xu, W. Han, P. Yang, T. Jia, S. Dong, H. Bi, A. Gulzar, D. Yang, S. Gai, F. He, Adv. Funct. Mater. 28 (2018) 1803804.